Supplementary Information (SI) for Journal of Materials Chemistry A.
This journal is © The Royal Society of Chemistry 2025

Electronic Supplementary Information (ESI)

for

Intrinsic proton relay in poly-phosphamide to bolster proton-exchange membrane fabrication and electrocatalytic proton reduction

Anup Mahata,[a] Laxmikanta Mallick,[a] Isha Mehta[b], Nidhi Kumari,[a] Sagarika Bhattacharya,[b]* and Biswarup Chakraborty,[a]*

[a]Department of Chemistry, Indian Institute of Technology Delhi, Hauz Khas, 110016, New Delhi, India.***cbiswarup@chemistry.iitd.ac.in**

[b]Department of Chemistry, National Institute of Technology Raipur, Raipur, Chhattisgarh, 492010, India.

Email: **sbhattacharya.chy@nitrr.ac.in**

Table of Contents

Materials and Methods

Materials used

The following chemicals; ethylene diamine (Spectrochem, 97 %), Tris(2-aminoethyl)amine (Sigma Aldrich, 98%), phenylphosphinic dichloride ($PhPOCl_2$, PPPC, 97%, Thermo Scientific), triethylamine (Et_3N, Induschembio, 99%), Toluene (Actylis), Diethyl ether (Finar), Ethanol (CHF chemicals, 99%), Formaldehyde (HCHO, Qualigens), Sulfuric acid (H_2SO_4, Qualigens), were purchased and used as received. Toluene was dried over sodium and benzophenone to be used for the synthesis of precursor phosphine oxide. The carbon cloth was purchased from RVL Scientific, India, and used after washing as explained below. The Carbon cloth electrode and Pt wire were used as working and reference electrodes, respectively, and were supplied by CHI, India. $Hg/HgSO_4$ and Ag/AgCl electrodes were purchased from Phadke Instruments, India. Nafion 117 containing solution was purchased from Sigma Aldrich.

Instrumental Methods.

Powder X-ray diffraction (PXRD). A BRUKER D8 Advance with Cu-$K_{\alpha 1}$ (λ = 1.5406 Å) source instrument was used to characterize the synthesized materials and obtain the PXRD diffractogram.

Thermogravimetric Analysis (TGA). The Pyris Diamond TGA/DSC/DTA (Perkin Elmer Instruments) in N_2 atmosphere was used to characterize the synthesized polymers using the TGA technique.

Dynamic light scattering (DLS). The Malvern Zetasizer, NANO ZS90 (Malvern Instruments Limited, U.K.) was used for the measurement of hydrodynamic diameter from DLS study of a DMSO dispersed solution of PPA-2, PPA-1a, and PPA-1b. A 4 mw He-Ne laser with an operating wavelength of 633 nm was connected to the instrument. The measurements were carried out in a glass cuvette at 25 ^{o}C with a scattering angle of 90 ^{o}.

Scanning electron microscopy (SEM). The TESCAN and model Magna Prime integrated with an EDX detector (Oxford make EDS) was used to collect SEM images. The EDS consists of an LN2-free SDD X-max 80 EDS detector. The as-synthesized powdered polymeric samples were directly observed over copper tape.

X-ray photoelectron spectroscopy (XPS). The X-ray photoelectron spectroscopy (XPS) technique was used for the surface chemical analysis. The measurement was done using ESCA+, Omicron nanotechnology, Oxford Instrument Germany, equipped with an aluminium monochromator with aluminium source (Al Kα radiation hν = 1486.7 eV). An operational voltage of 15kV and current of 15mA was applied in the instrument.

^{13}C CPMAS NMR (Cross Polarization Mass Angle Spinning Nuclear Magnetic Resonance) analysis. A 400 MHz JEOL NMR instrument with Topspin software was used to analyze the as-synthesized specimen. For further analysis of the recorded data, MestReNova software was used to analyze the spectra. The earlier reported literature was used to assign the chemical shift values and analysed accordingly.

Small-angle X-ray Scattering (SAXS) study. The Anton Paar SAXS point 2.0 apparatus outfitted with a Primux 100 micro microfocus Cu X-ray source and point collimation was used collect small angle X-ray scattering data. A 2D EIGER R series hybrid phonon counting (HPC) detectors having an HR WAXS module was equipped with the instrument. The sample was measured in Scotch tape having a distance the sample and the detector is 850.0 mm, and the exposure unit temperature was 296.1 K. A q range of 0 to 3 nm^{-1} was used to record the SAXS data, where θ is half of the scattering angle, λ is the wavelength, which in this case was 1.54 Å and where $q = (4\pi \sin\theta/\lambda)$ corresponds to the modulus of the scattering vector. The scattering was measured over a total of two 30-minute frames after the sample was subtracted from the background for the analysis.

Small angle X -ray scattering was collected on the Anton Paar SAXS point 2.0 apparatus outfitted with a Primux 100 micro microfocus Cu X-ray source and point collimation. The instrument is equipped with 2D EIGER R series hybrid phonon counting (HPC) detectors with an HR WAXS module. The distance between the sample and the detector is 850.0 mm. The sample was measured in Scotch Tape. The scattering was measured over a total of two 30-minute frames after the sample was subtracted from the background for the analysis. The SAXS data was recorded with a q range of 0 to 3 nm-1, where $q = (4\pi \sin\theta/\lambda)$ corresponds to the modulus of the scattering vector, θ is half of the scattering angle and λ is the wavelength, which in this case was 1.54 Å. The exposure unit temperature was 296.1 K. The sample was subtracted from the background for the analysis. A

detailed Guinier analysis was performed at a low q region of 0.002–0.002 Å and fitting was carried out using RAW software following the Guinier approximation (1) and the pair distance distribution functions (PDDF) was determined by using the equation (2) by the indirect Fourier Transform (IFT) method within the RAW software.

$$\ln[I(Q)] = \ln[I(0) - \frac{Q^2 Rg^2}{3} \quad (1)$$

$$R(r) = \frac{r}{2\pi^2}\int_0^\infty I(Q)Qsin(Qr)dQ \quad (2)$$

BET analysis. The BELSORP-maxII (BELSORP – series) from Microtrac BEL Corp and Quantachrome Instruments NOVA 2000 multi-station nitrogen sorption analyzer standard model version 11.03 was used to carry out, N_2 adsorption-desorption isotherm and pore size distribution measurements. The samples were degassed at 120 ℃ for 12h prior to the analysis in the cells of BET instrument and analysis was carried out using liquid nitrogen. The SABET was calculated by data fitting of nitrogen sorption to BET model in the relative pressure range of 0.01 to 1.0. The average pore diameter and pore size distribution was estimated using Barrett-Joyner-Halenda (BJH) model for pore size and volume analysis.

Computational Studies. The Gaussian 09 software was used to record density functional theory (DFT) calculations. The ground state configurations of the simplified phosphamide functionality was optimized by employing B3LYP functional in combination with Becker's hybrid exchange functional, Lee-Yang-Parr nonlocal correlation functional and 6-311(g) basis set. The frequency calculations were performed to identify and characterize the potential energy of each stationary point on the surface. The optimized and equilibrated structures obtained from Mulliken charge density (M.C.D.) was further calibrated for population analysis using natural bond orbitals (NBO) method by utilizing the wave functions from B3LYP/6-311(g) level. The objective of NBO analysis was to identify and quantify charge transfer interaction from intermolecular orbital interactions which involves considering all possible potential interactions between empty acceptor

NBOs and filled donor NBOs. In order to signify the contribution of these interactions towards energy stabilization, the stabilization energy from the second order perturbation theory is employed.

To ascertain the degree of electronic interaction and its influence on the overall molecule stability, the stabilization energy E (2) corresponding to each electron delocalization between each donor NBO (i) and acceptor NBO (j) is calculated following the below formula:

$$E^{(2)} = q_i \frac{(F_{i,j})^2}{\varepsilon_j - \varepsilon_i}$$

Where, q_i corresponds to the occupancy of donor orbital, ε_i, ε_j are the diagonal elements corresponding to the orbital energies, and F_i, j is the off-diagonal NBO Fock matrix element.

Mechanical properties measurements. The tensile strength of the membranes was measured using a universal test machine (Zwick/Roell, Model: Z010; Germany) at a loading rate of 50 mm/min according to ASTM D638 (Type-V), and force–displacement data was recorded. For the evaluation, tensile strength, stretchability, and moduli were recorded, and a series of 3 sample membranes were tested for each case.

Water swelling experiments.

Water Uptake (%WU) measurements. The gravimetric change of PPA-2/PVA, and PPA-2/PMMA films by immersing them in water was used to test the water swelling properties. The weight of dry films was measured and then dipped into distilled water. The films were immersed in a distilled water a period of 24 h at room temperature. The water-soaked PVA and PMMA composite films were scrubbed and was weighed accordingly to calculate % water uptake. The water uptake of PPA-2/PVA, and PPA-2/PMMA films was calculated using the following formula:

$$\boldsymbol{WU\ (\%) = [\Delta W/W_{dry}]\ X\ 100}$$

Here, ΔW is the increased weight of films because of water absorption, and W_{dry} is the weight of dry films.

Swelling ratio (%SR) measurements.

Similarly, the water uptake of PPA-2/PVA, and PPA-2/PMMA films was calculated using the following formula:

$$SR\ (\%) = [\Delta L/L_{dry}]\ X\ 100$$

where the increase in length due to water absorption is ΔL and the length of the dry membrane is L_{dry}.

Oxidative stability experiments. The oxidative resistance was assessed with 10 × 10 mm^2 dimensions of membranes by heating the membrane samples in Fenton's solution (3% aq. H_2O_2, 2 ppm of $FeSO_4$ solution), and the time necessary for complete dissolution in Fenton's solution was reported as oxidative stability. A series of PPA-2/PVA and PPA-2/PMMA based 10 × 10 mm^2 membrane samples were heated for 24 h with a time interval of 6 h. The collected membranes from Fenton's solution were washed with distilled water and dried in a vacuum oven for 12 h before capturing FESEM image.

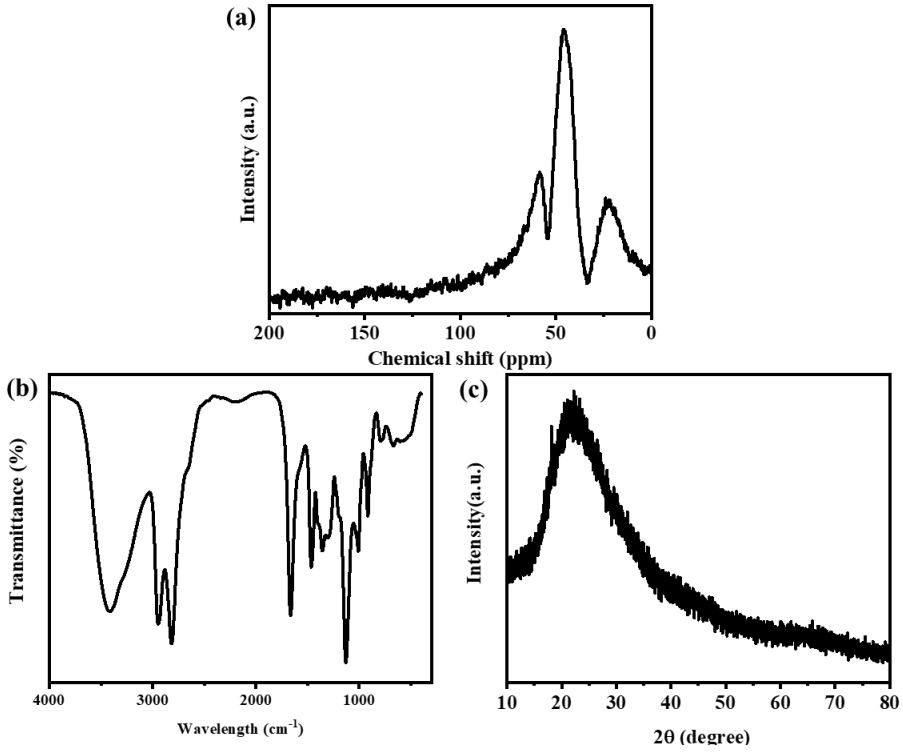

Figure S1. (a) ^{13}C CP-MAS NMR spectrum of PPA-1b, (b) FTIR spectra of the PPA-1b, (c) PXRD analysis of the PPA-1b.

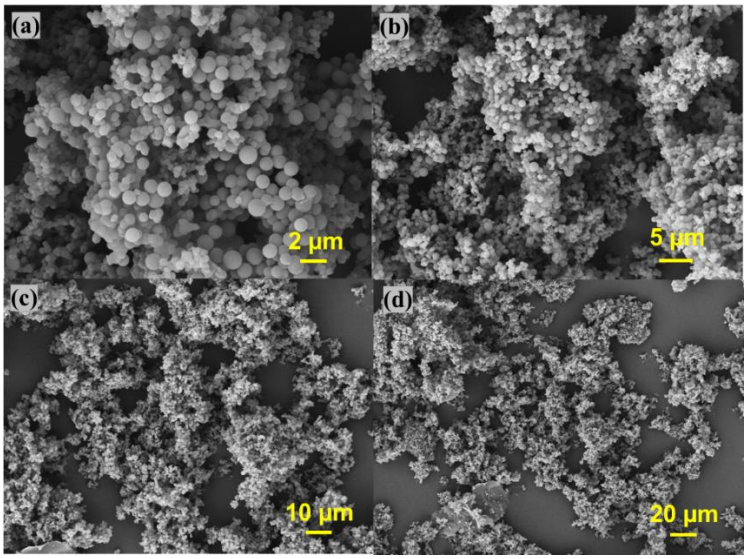

Figure S2. (a-d) FESEM image of PPA-1b at diiferent magnification.

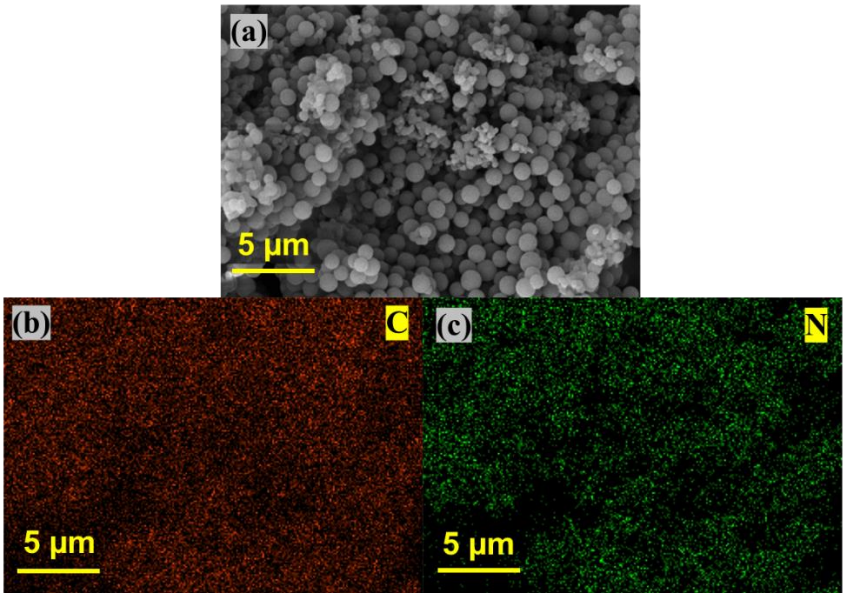

Figure S3. (a) FESEM image of a selected area of the PPA-1b and corresponding EDX elemental mapping for (b) C and (c) N.

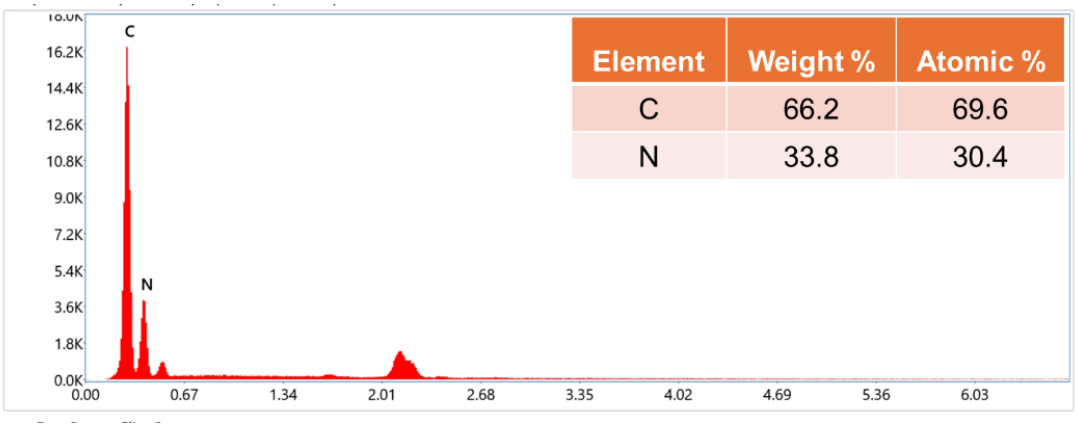

Element	Weight %	Atomic %
C	66.2	69.6
N	33.8	30.4

Figure S4. EDX spectrum of as-synthesized PPA-1b (Inset: the weight and atomic percentage of the present elements in PPA-1b).

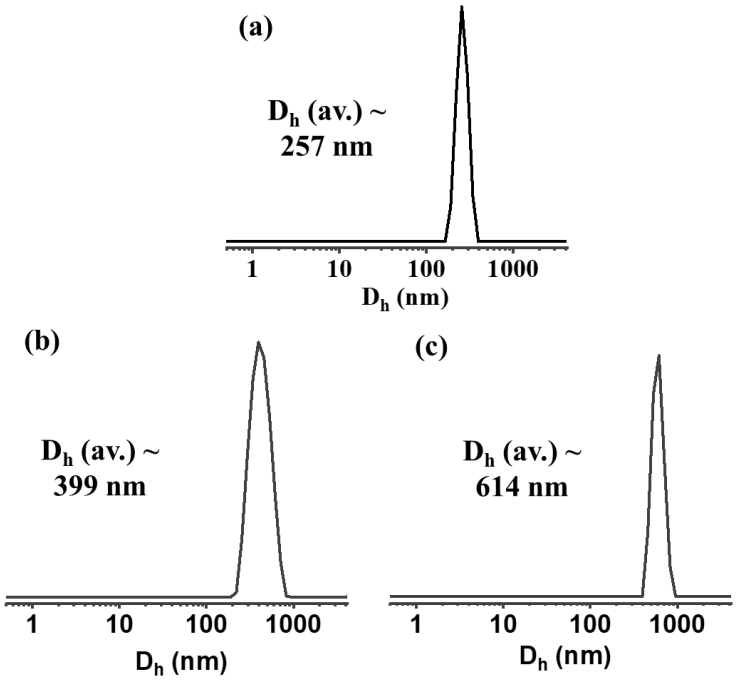

Figure S5. DLS study with a solution of catalysts dispersed in dimethyl sulfoxide (DMSO) for (a) PPA-2, (b) PPA-1a, and (c) PPA-1b.

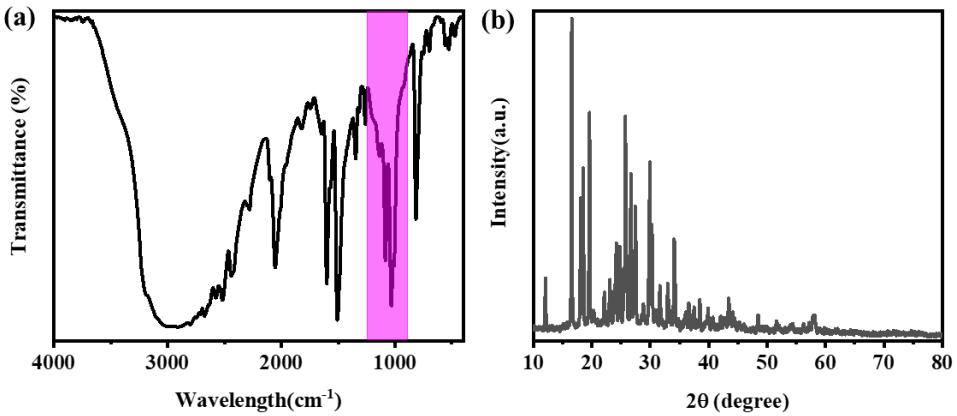

Figure S6. (a) FTIR spectrum, and (b) PXRD analysis of PPA-2.

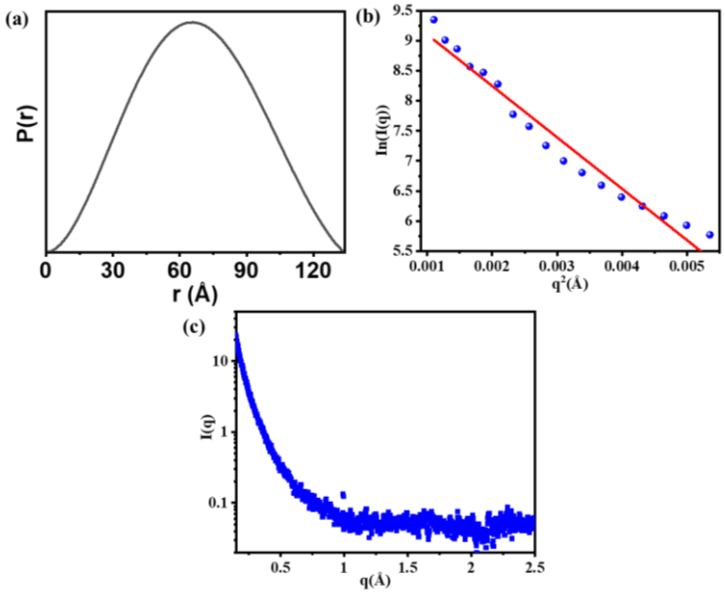

Figure S7. (a) Pair distance distribution function obtained for PPA-2 from the SAXS study, (b) The plot of the ln(I(q)) versus q^2 in the Guinier region for PPA-2. The presence of non-linearity in the linear fit highlights the formation of aggregation. The data shown in the blue filled circle, the linear fitting shown in the red solid line, and Guinier fits performed within the ranges of $q_{max}*R_g$ = 1.22 to $q_{min}*R_g$ = 0.51, and (c) Plot showing the scattering intensity, I(q), as a function of the scattering vector, q (the data points: blue) for PPA-2.

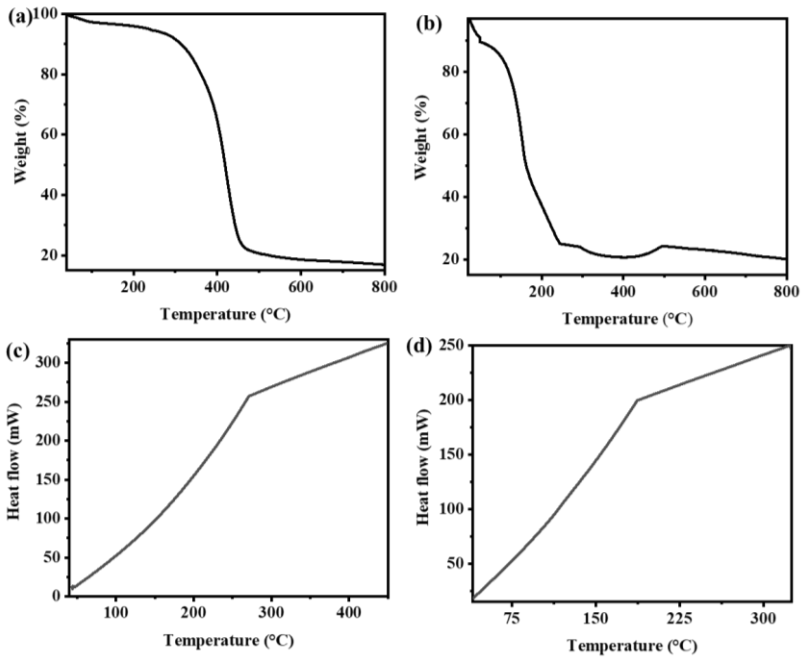

Figure S8. (a) TGA plot of the PPA-1a, (b) PPA-1b. DSC plot of (c) PPA-1a, and (d) PPA-1b.

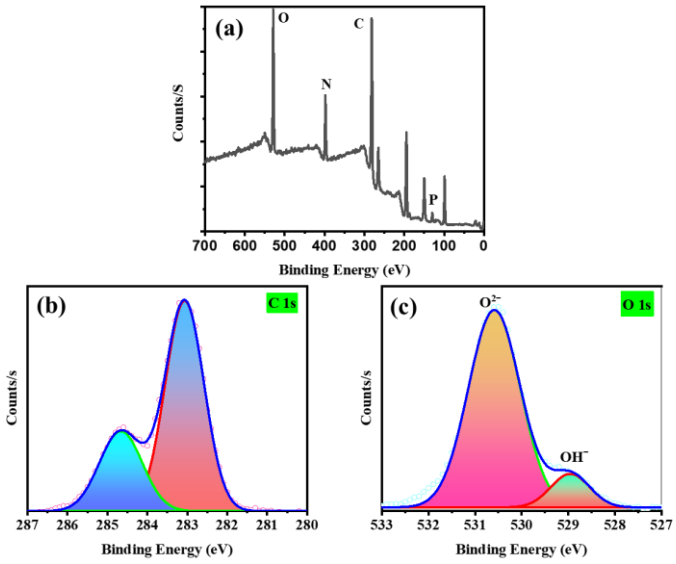

Figure S9. X-ray photoelectron spectrum (XPS) of PPA-2: (a) complete elemental survey scan. Deconvolution of core-level (b) C 1s, and (c) O 1s.

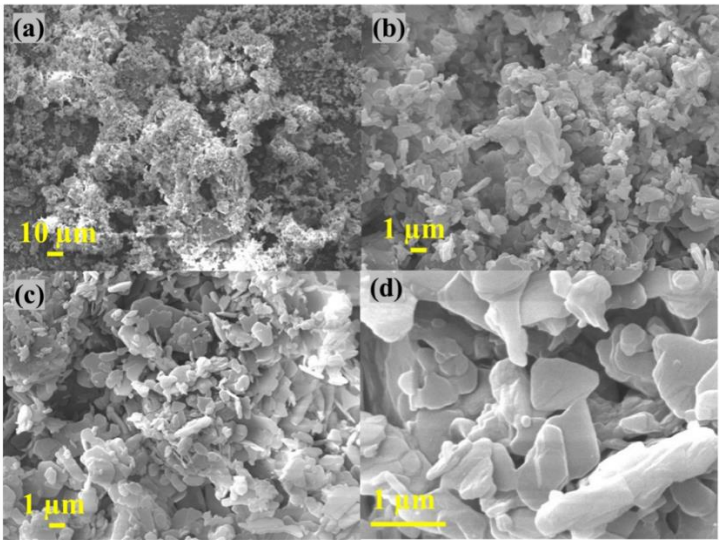

Figure S10. FESEM images of the PPA-2 at different magnifications.

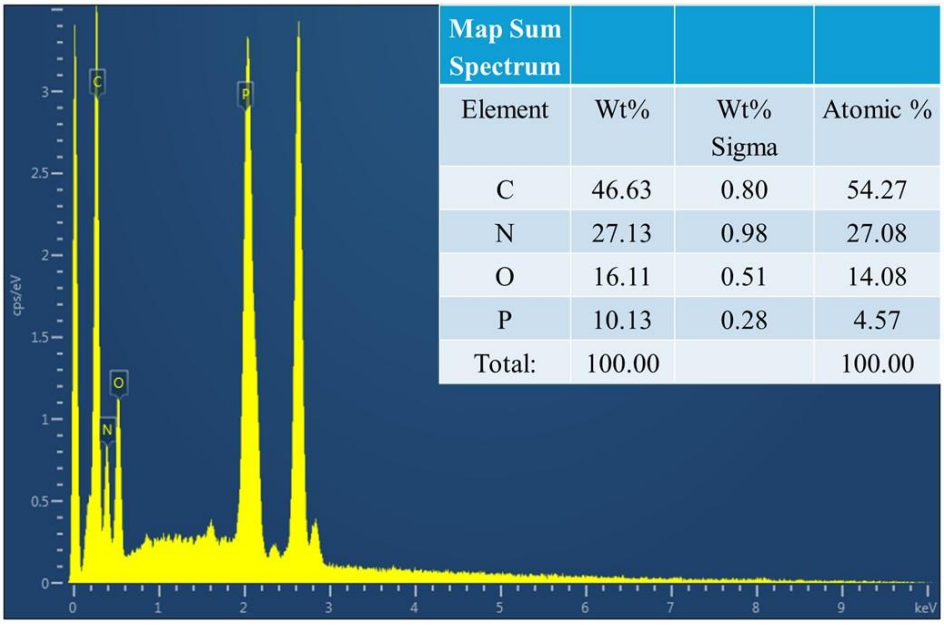

Map Sum Spectrum			
Element	Wt%	Wt% Sigma	Atomic %
C	46.63	0.80	54.27
N	27.13	0.98	27.08
O	16.11	0.51	14.08
P	10.13	0.28	4.57
Total:	100.00		100.00

Figure S11. EDX spectra of as-synthesized PPA-2 (Inset: the weight and atomic percentage of the present elements in PPA-2).

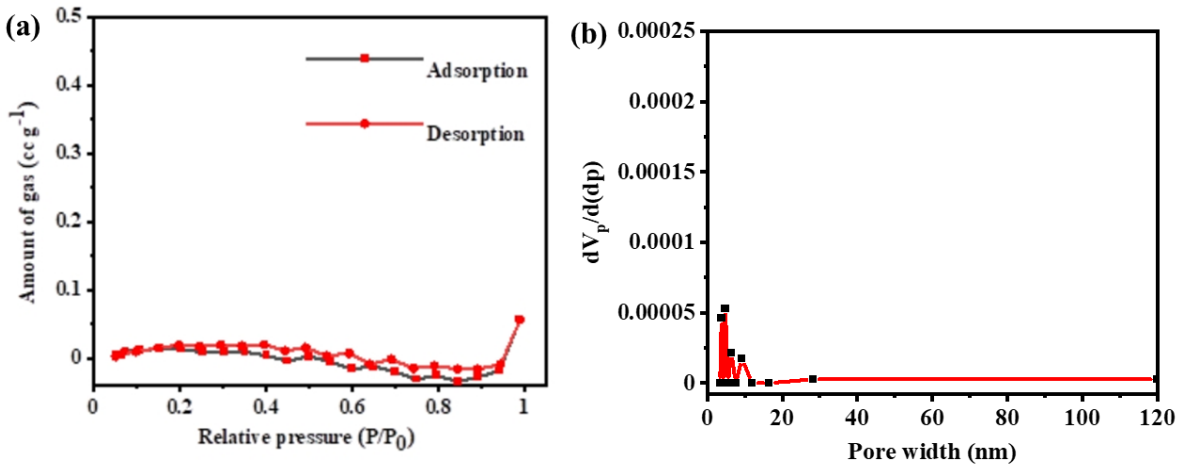

Figure S12. (a**)** N_2 sorption isotherm of PPA-1a measured at 77 K, and (b) Pore size distribution (PSD) curve from desorption study of PPA-1a measured using the BJH model.

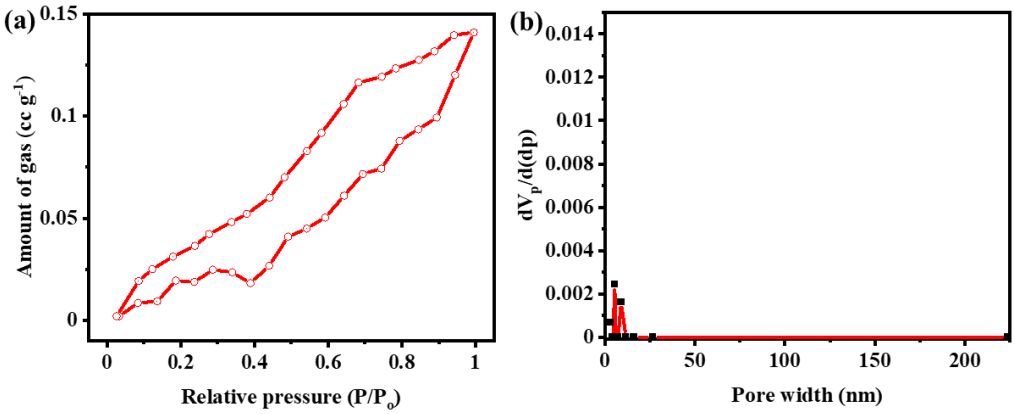

Figure S13. (a) N_2 sorption isotherm of PPA-1b measured at 77 K, and (b) Pore size distribution (PSD) curve from desorption study of PPA-1b measured using the BJH model.

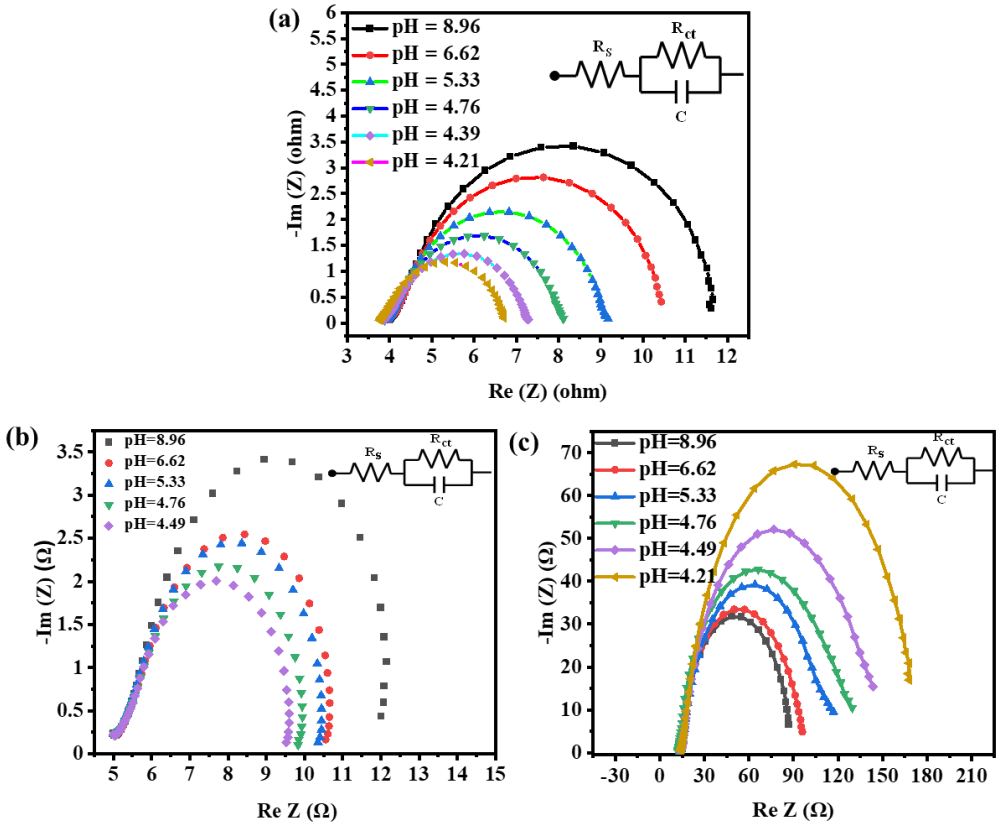

Figure S14. Nyquist plots recorded at various pH using (a) PPA-2, (b) PPA-1a, and (c) PPA-1b.

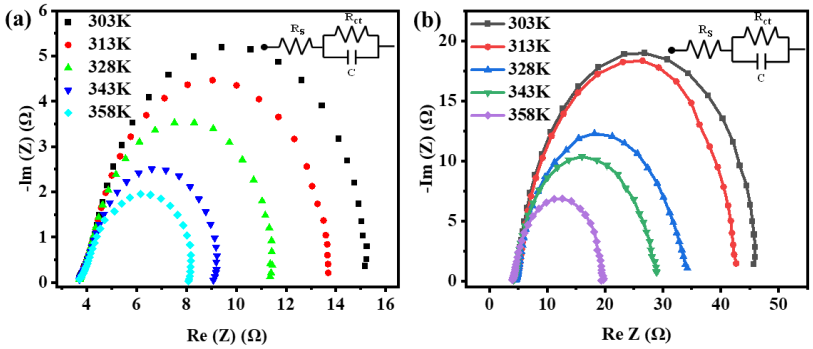

Figure S15. Nyquist plots are recorded at different temperatures for (a) PPA-1a, and (b) PPA-1b.

Table S1. Proton conductivity measurement of PPA-1a, PPA-1b, and PPA-2 at various pH.

Sample	PPA-1a		PPA-1b		PPA-2	
pH	$R_s(\Omega)$	σ (S cm^{-1})	$R_s(\Omega)$	σ (S cm^{-1})	$R_s(\Omega)$	σ (S cm^{-1})
7.96	4.07	3.28×10^{-3}	4.12	2.08×10^{-4}	4.01	3.57×10^{-3}
6.62	4.02	3.89×10^{-3}	3.99	2.47×10^{-4}	3.93	4.51×10^{-3}
5.33	3.96	4.78×10^{-3}	3.92	2.72×10^{-4}	3.91	4.92×10^{-3}
4.49	3.92	5.91×10^{-3}	3.84	3.11×10^{-4}	3.88	6.23×10^{-3}
4.21	3.83	7.33×10^{-3}	3.71	4.33×10^{-4}	3.77	8.53×10^{-3}

Table S2. Proton conductivity measurement of PPA-1a, PPA-1b and PPA-2 at various temperatures.

Sample	PPA-1a		PPA-1b		PPA-2	
pH	$R_s(\Omega)$	σ (S cm^{-1})	$R_s(\Omega)$	σ (S cm^{-1})	$R_s(\Omega)$	σ (S cm^{-1})
303	3.82	2.11×10^{-3}	3.69	2.831×10^{-4}	3.77	6.57×10^{-3}
313	3.76	2.51×10^{-3}	3.62	3.424×10^{-4}	3.71	1.019×10^{-2}
323	3.71	3.27×10^{-3}	3.56	4.302×10^{-4}	3.66	1.287×10^{-2}
333	3.63	4.66×10^{-3}	3.48	9.337×10^{-2}	3.59	1.86×10^{-2}
343	3.58	6.91×10^{-3}	3.43	1.345×10^{-3}	3.51	2.405×10^{-2}
353	3.51	8.21×10^{-3}	3.38	1.746×10^{-3}	3.44	3.146×10^{-2}
358	3.43	1.051×10^{-2}	3.34	1.971×10^{-3}	3.37	4.703×10^{-2}

Table S3. Comparative table of some recently reported materials for the performance of proton conductivity.

Materials	Conditions	E_a (eV)	Conductivity (S cm^{-1})	References
PPA-1a	85 °C	0.14	1.3×10^{-2}	This work
PPA-1b	85 °C	0.58	1.97×10^{-3}	This work
PPA-2	85 °C	0.12	4.7×10^{-2}	This work
Ni-MOF-74	80 °C	-	1.4×10^{-4}	1
HKUST-1	25 °C	-	1.5×10^{-5}	2
PAES	80 °C	-	7.5×10^{-3}	3
TPOP	85 °C	0.285	2.5×10^{-2}	4
SPP-4	100 °C	-	8.8×10^{-2}	5
PAAM	183 °C	0.24	5.25×10^{-2}	6
PNVP	180 °C	0.11	1.52×10^{-1}	7
IITKGP-101	80 °C	0.78	2.45×10^{-4}	8
ImH-2D	95 °C	0.31 eV	3.2×10^{-2}	9
PEEK	80 °C	-	19.8×10^{-3}	10
SmPPES	80 °C	0.103	1.1×10^{-1}	11
PI	140 °C	0.42	5.6×10^{-2}	12
FSPAE	80 °C	-	6.2×10^{-2}	13
PTDPBSH	90 °C	-	15.2×10^{-2}	14
Tb-TTHA	60 °C	0.68	2.57×10^{-2}	15
Mg_2(dstp)	80 °C	0.19	1.3×10^{-4}	16

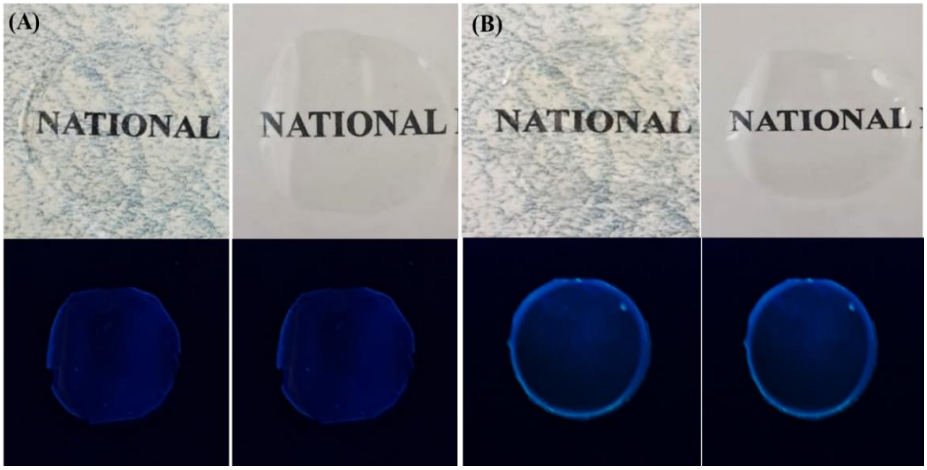

Figure S16. (A) PMMA/DMF and (B) PVA/H_2O; control film on two different surfaces under daylight and under 365 nm UV light.

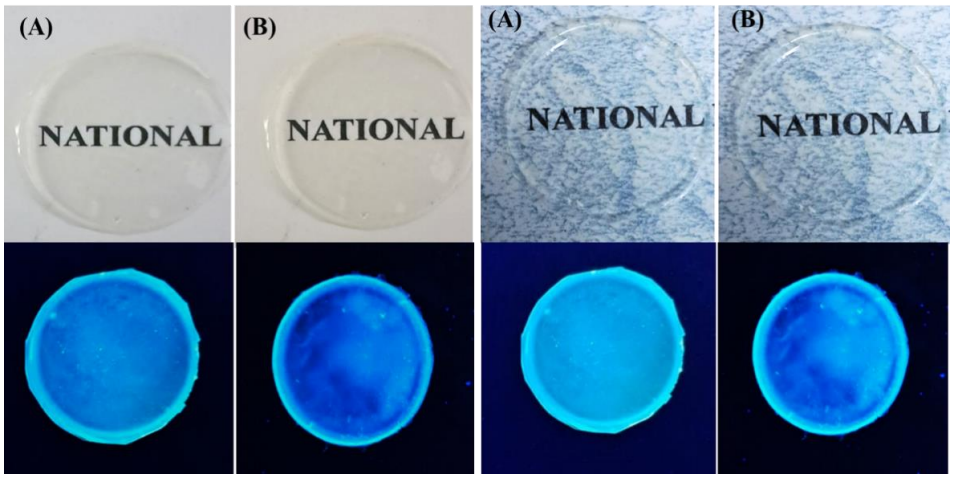

Figure S17. (A) PPA-2/PVA polymer (B) PPA-2/PMMA polymer under daylight (white background) and 365 nm UV light (black background). Four images provide in right side are taken on the on the rough background to showcase the film.

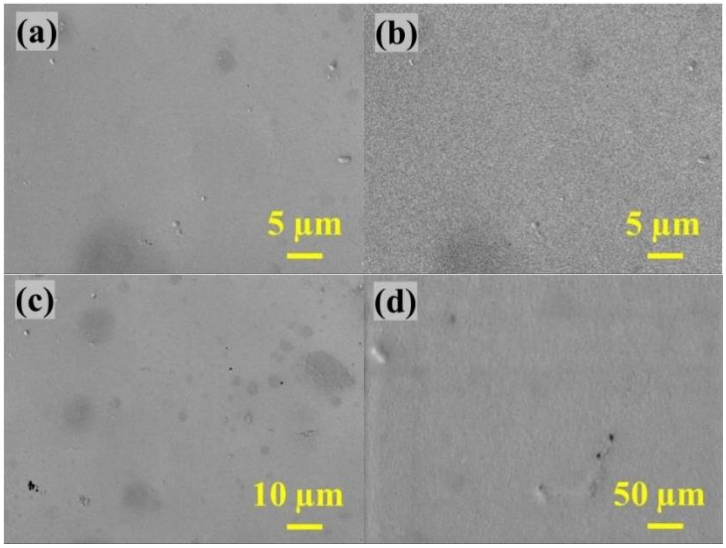

Figure S18. FESEM images at different magnification for PPA-2/PMMA membrane before proton permeability test.

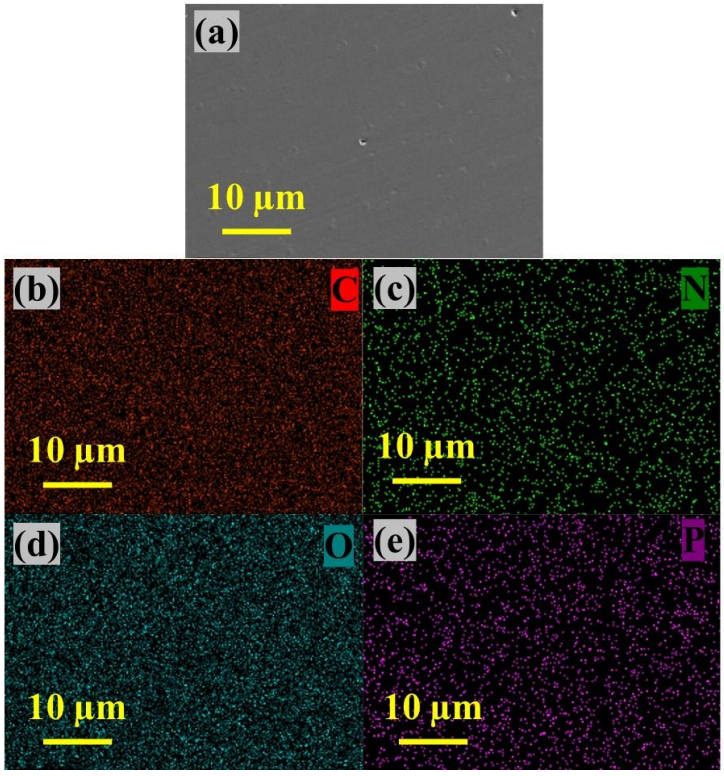

Figure S19. FESEM image of a selected area of the PPA-2/PVA membrane and corresponding EDX elemental mapping for (b) C, (c) N, (d) O, and (e) P before proton permeability test.

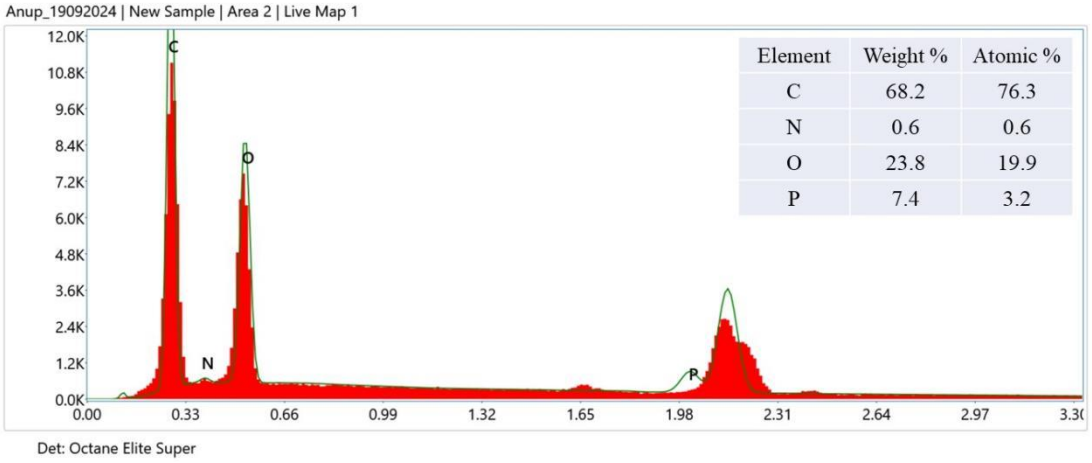

Element	Weight %	Atomic %
C	68.2	76.3
N	0.6	0.6
O	23.8	19.9
P	7.4	3.2

Figure S20. EDX spectra of as-synthesized PPA-2/PVA membrane. Inset: the weight and atomic percentage of the present elements in the membrane before proton permeability test.

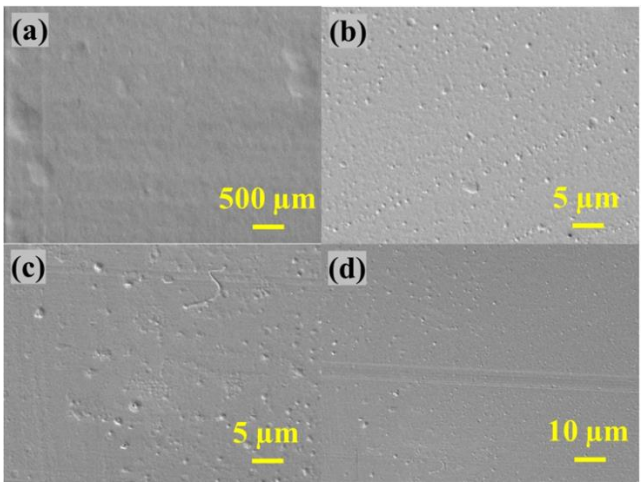

Figure S21. FESEM images at different magnification for PPA-2/PMMA membrane before proton permeability test.

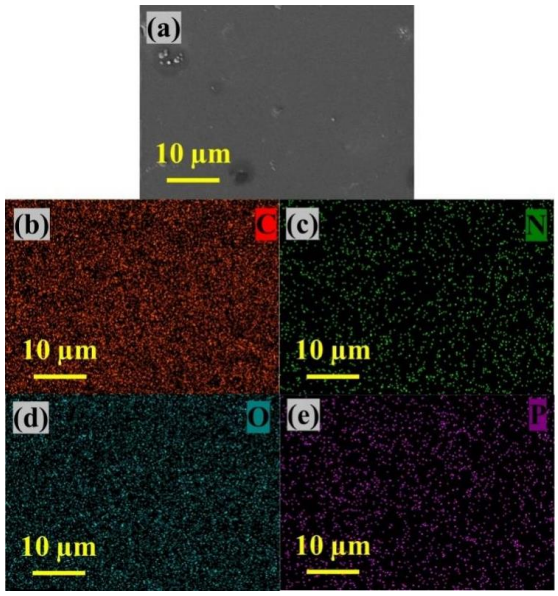

Figure S22. FESEM image of a selected area of the PPA-2/PVA membrane and corresponding EDX elemental mapping for (b) C, (c) N, (d) O, and (e) P before proton permeability test.

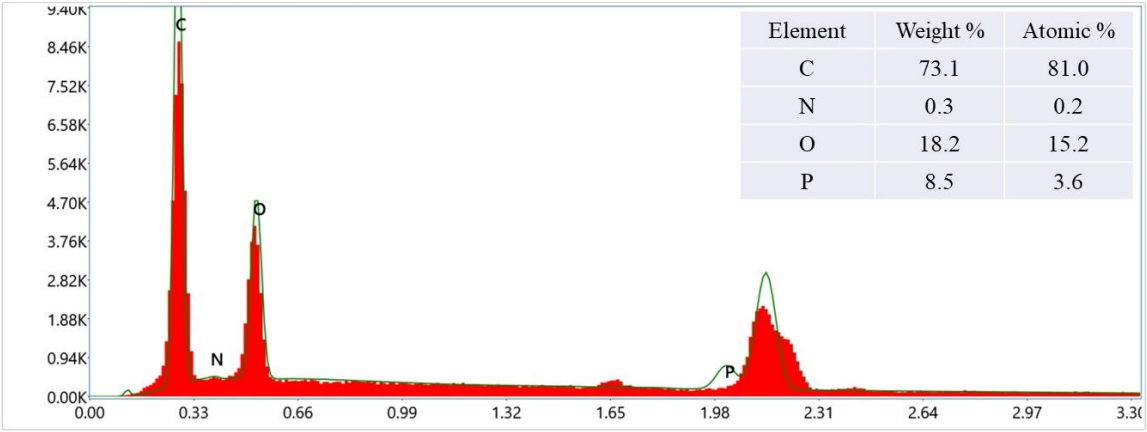

Figure S23. EDX spectra of as-synthesized PPA-2/PMMA membrane. Inset: the weight and atomic percentage of the present elements in the membrane before proton permeability test.

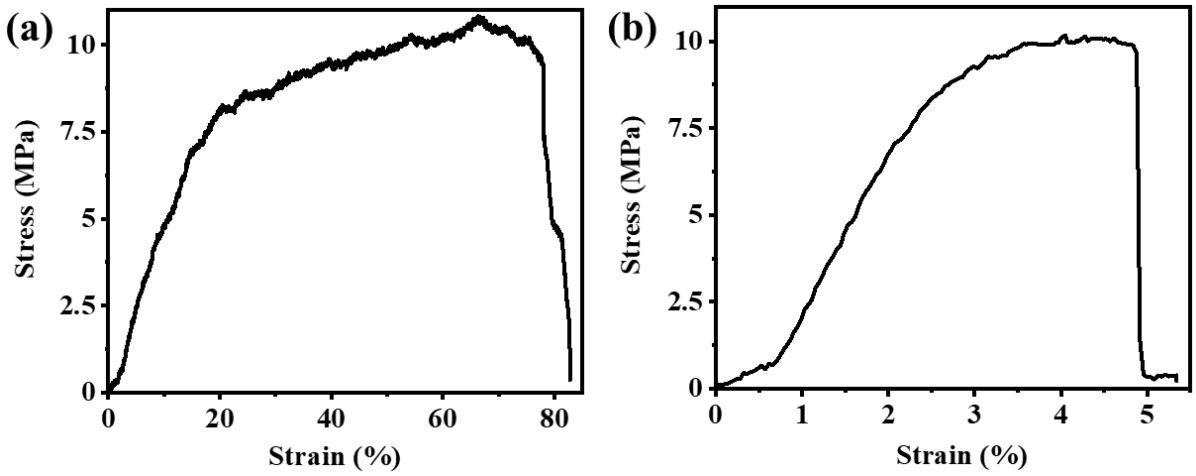

Figure S24. Stress-strain plot for the mechanical properties of (a) PPA-2/PVA films, and (b) PPA-2/PMMA films.

Table S4. Comparison of mechanical properties and water swelling of PPA-2/PVA and PPA-2/PMMA film at room temperature.

Films	Tensile strength (MPa)	Elongation at break (%)	Young modulas (GPa)	Water uptake (%)	Swelling ratio (%)
PPA-2/PVA	10.9	83	0.5	37.3	17.1
PPA-2/PMMA	10.2	5	4.6	2.9	2.7

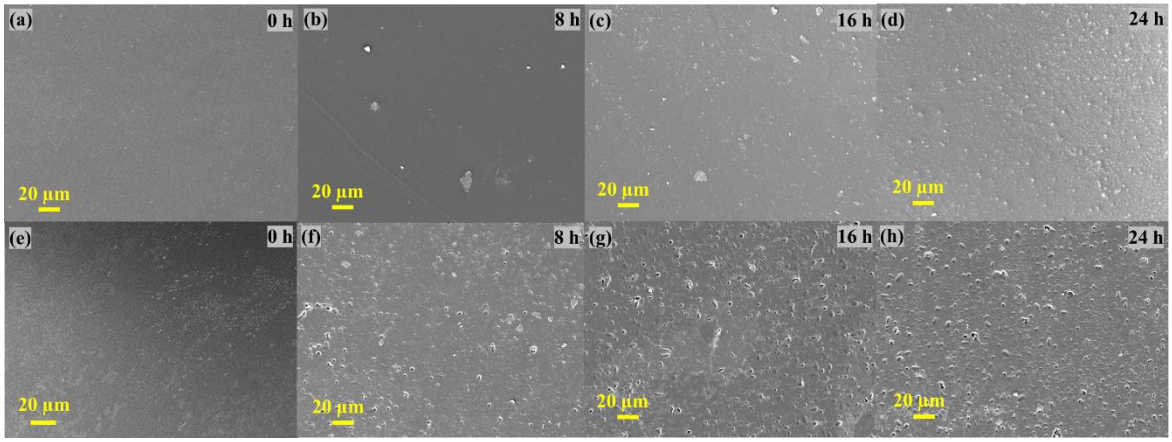

Figure S25. FESEM images (a-d) of PPA-2/PVA membranes over an interval of 8 h (τ = 0, 8, 16, 24 h), and (e-h) of PPA-2/PMMA membranes over an interval of 8 h (τ = 0, 8, 16, 24 h) in Fenton's solution.

Table S5. Proton permeability experiment with PPA-2/PVA and PPA-2/PMMA and PVA and PMMA films, and Nafion 117 membrane.

PVA/H_2O		PMMA/DMF		PPA-2/PVA		PPA-2/PMMA		Nafion 117	
Time	pH	Time	pH	Time	pH	Time	pH	Time	pH
0	7.47	0	7.48	0	7.51	0	7.54	0	7.56
1	7.41	1	7.42	1	7.42	1	7.44	1	7.37
2	7.36	2	7.37	2	7.31	2	7.33	2	6.72
3	7.29	3	7.32	3	7.20	3	7.24	3	6.13
4	7.24	4	7.28	4	7.11	4	7.13	4	5.61
5	7.23	5	7.25	5	6.81	5	7.02	5	5.27
10	7.17	10	7.14	10	6.33	10	6.61	10	4.81
15	7.11	15	7.09	15	5.73	15	6.29	15	4.52
30	6.95	30	7.04	30	4.17	30	5.16	30	3.86
45	6.89	45	7.01	45	3.52	45	4.47	45	3.09
60	6.84	60	6.98	60	2.89	60	3.88	60	2.37

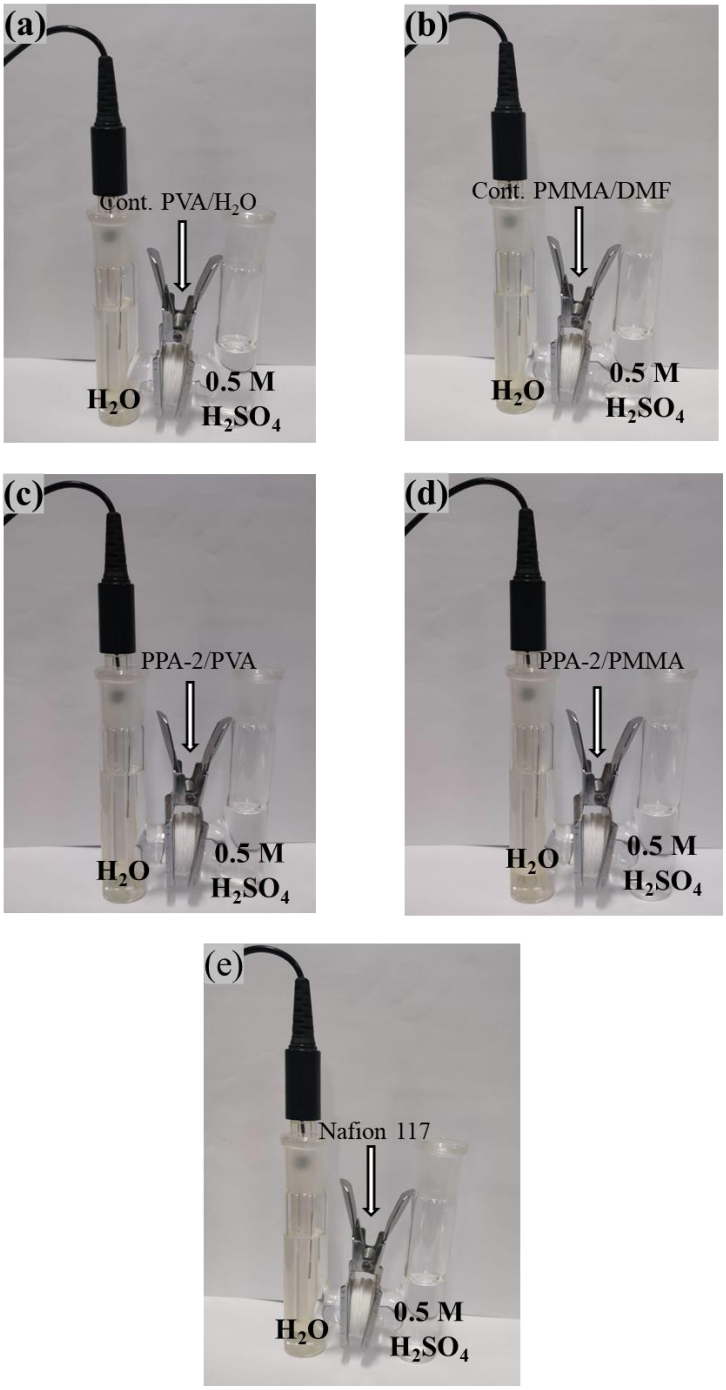

Figure S26. Experimental set-up of proton permeability measurements using` the diffusion cells with the (a-b) controlled PVA/H_2O and PMMA/DMF based membrane with (c-d) corresponding PPA-2 functionalized into the PVA/H_2O and PMMA/DMF based membranes, and Nafion 117 in different testing solutions having water and 0.5 M H_2SO_4 solution.

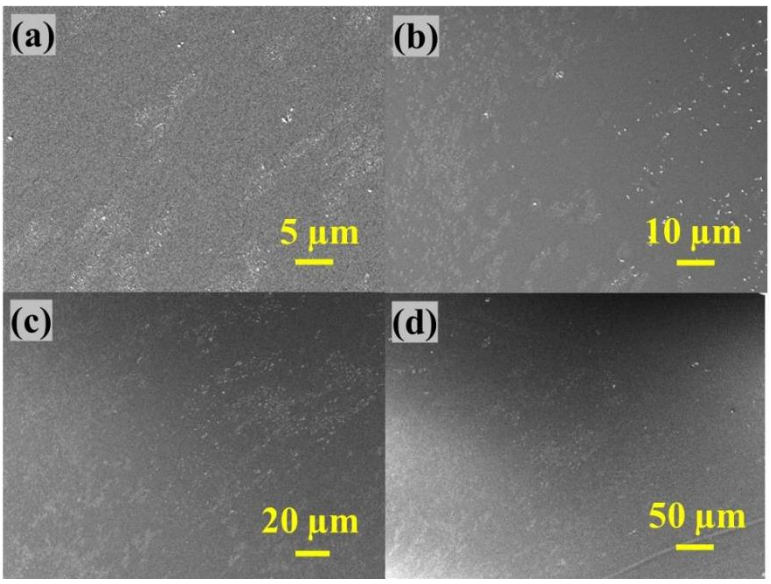

Figure S27. FESEM images at different magnification for PPA-2/PVA membrane after proton permeability test.

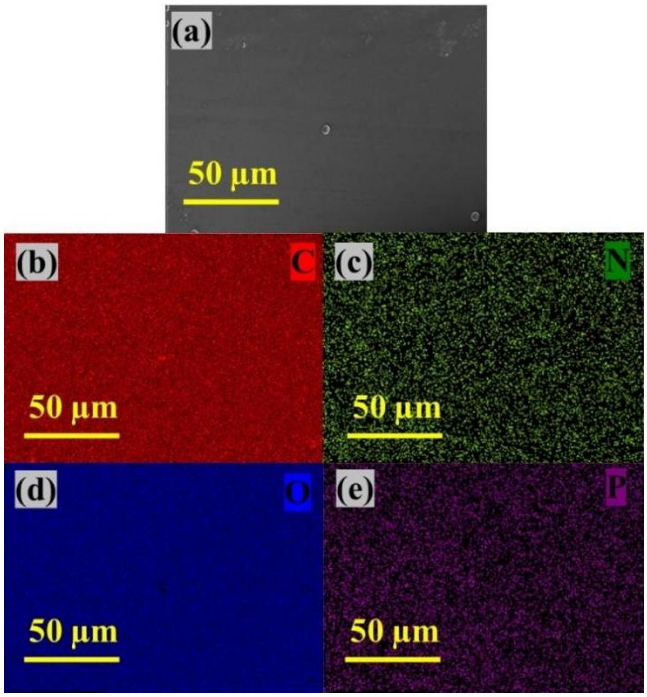

Figure S28. FESEM image of a selected area of the PPA-2/PVA membrane and corresponding EDX elemental mapping for (b) C, (c) N, (d) O, and (e) P after proton permeability test.

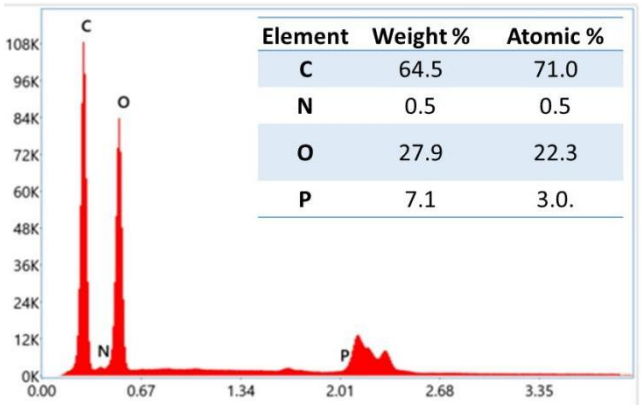

Figure S29. EDX spectra of as-synthesized PPA-2/PVA membrane. (Inset: the weight and atomic percentage of the present elements in the membrane after proton permeability test).

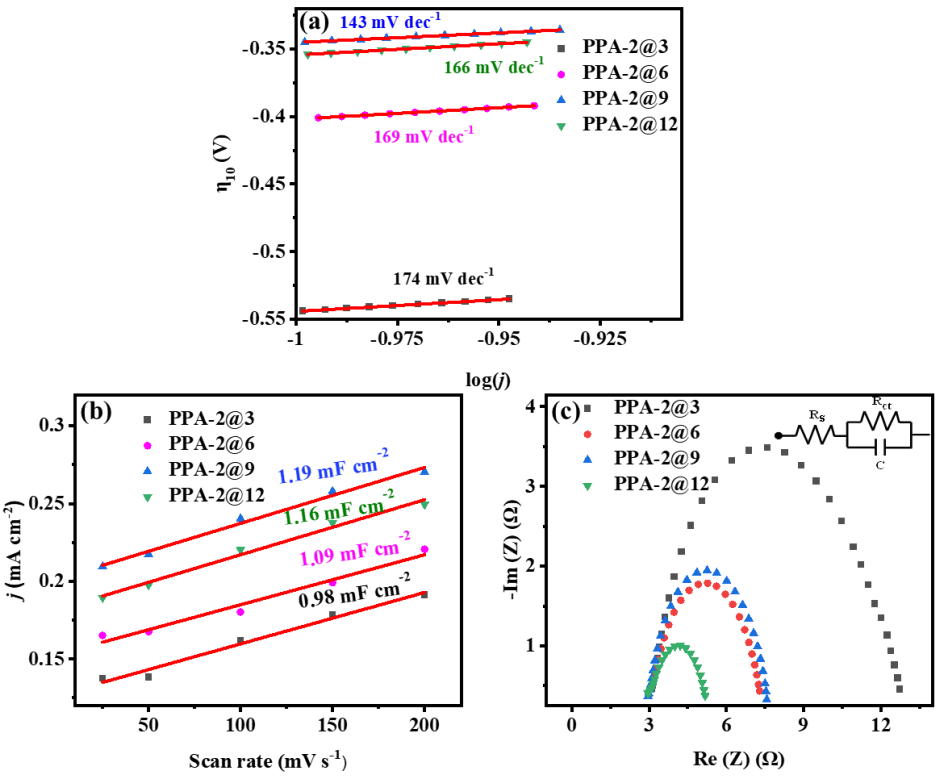

Figure S30. (a) Tafel slopes from the polarization curve (from LSV study in 0.5 M H_2SO_4, scan from 0 to -1.5 V vs $Hg/HgSO_4$ at a scan rate of 1 mV s^{-1}), (b) Fitting C_{dl} values and (c) Nyquist plots of CC and CC loaded with different amount of PPA-2 (in mg).

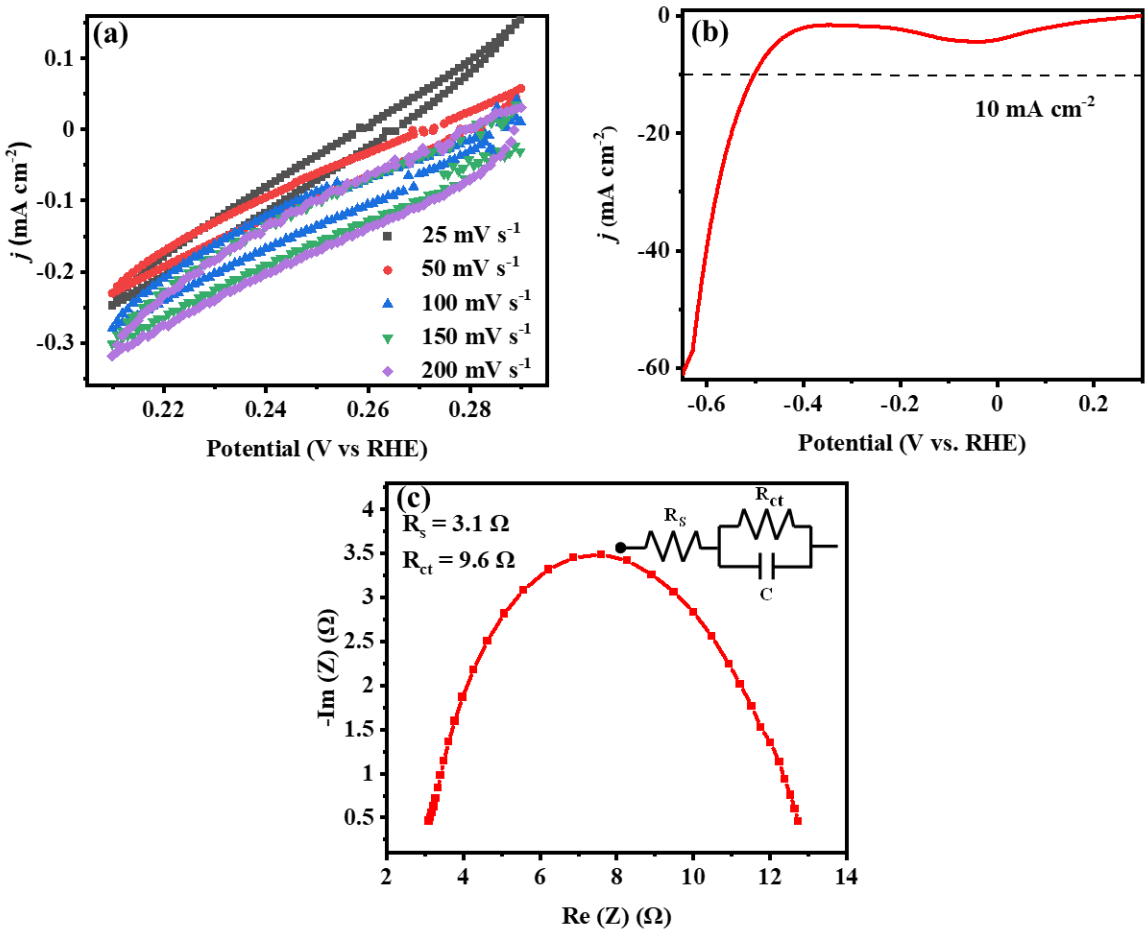

Figure S31. (a) Cyclic voltammetry (CV) at different scan rates (25, 50, 100, 150, and 200 mV s^{-1}) for ECSA and C_{dl} calculation, (b) Linear sweep voltammetry (LSV) curve and (c) Nyquist plot of PPA-2@3.

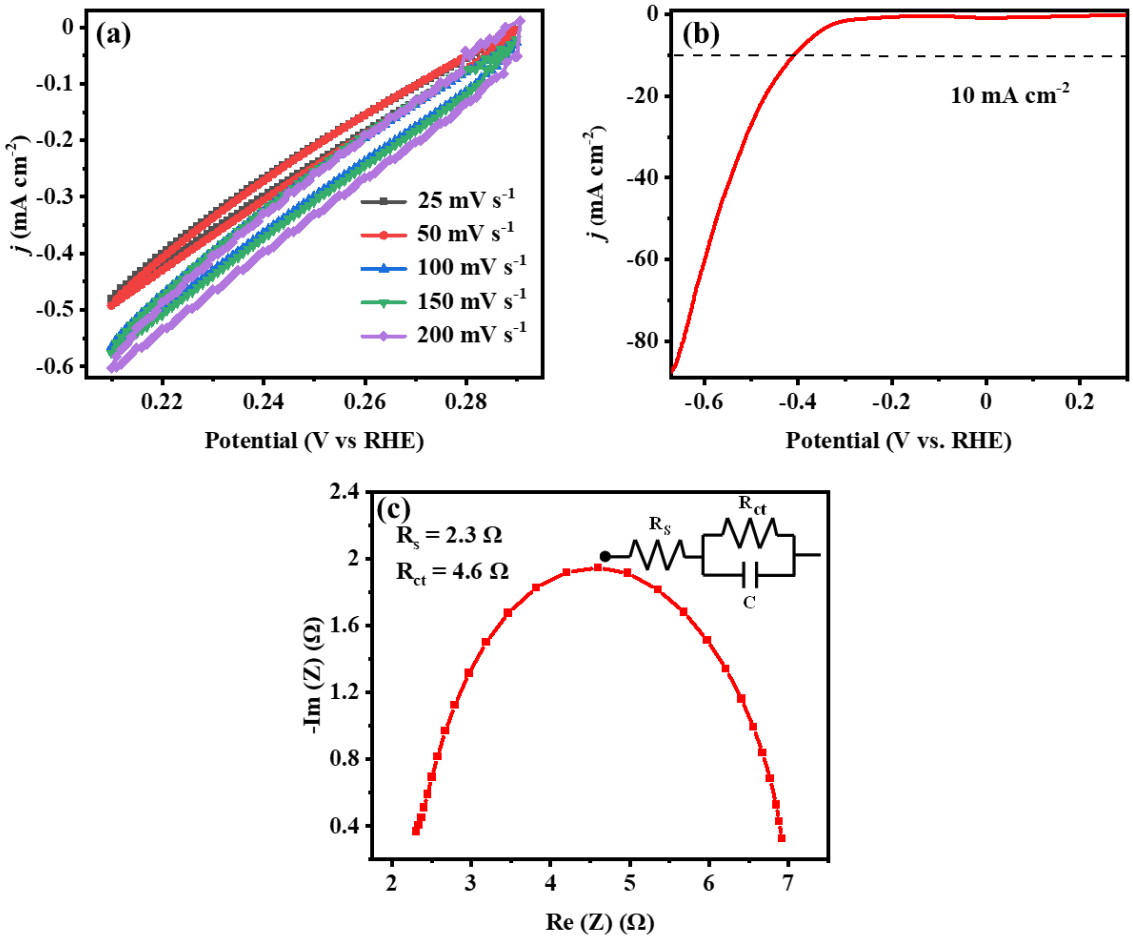

Figure S32. (a) Cyclic voltammetry (CV) at different scan rates (25, 50, 100, 150, and 200 mV s^{-1}) for ECSA and C_{dl} calculation, (b) linear sweep voltammetry (LSV) curve and (c) Nyquist plot of PPA-2@6.

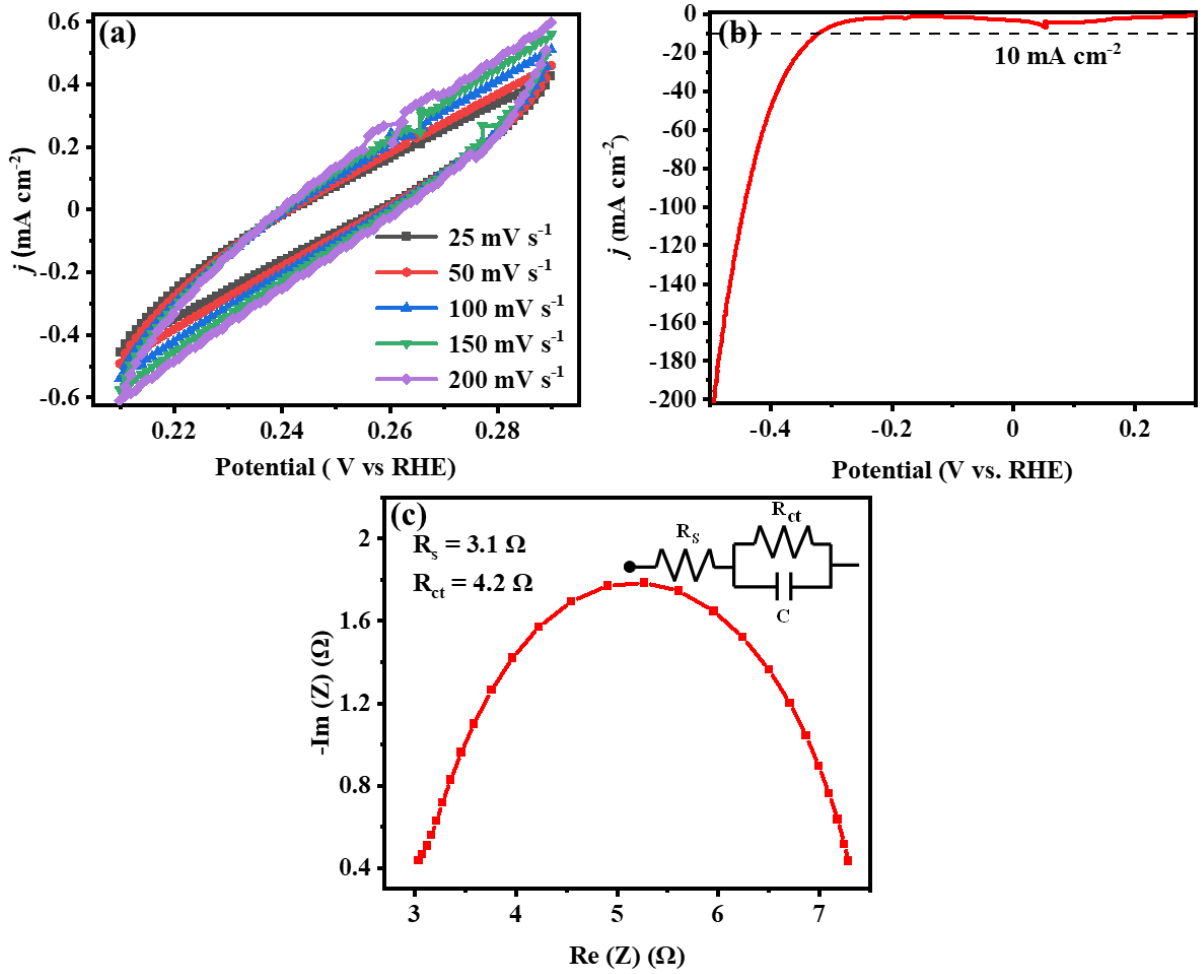

Figure S33. (a) Cyclic voltammetry (CV) at different scan rates (25, 50, 100, 150, and 200 mV s^{-1}) for ECSA and C_{dl} calculation, (b) linear sweep voltammetry (LSV) curve and (c) Nyquist plot of PPA-2@9.

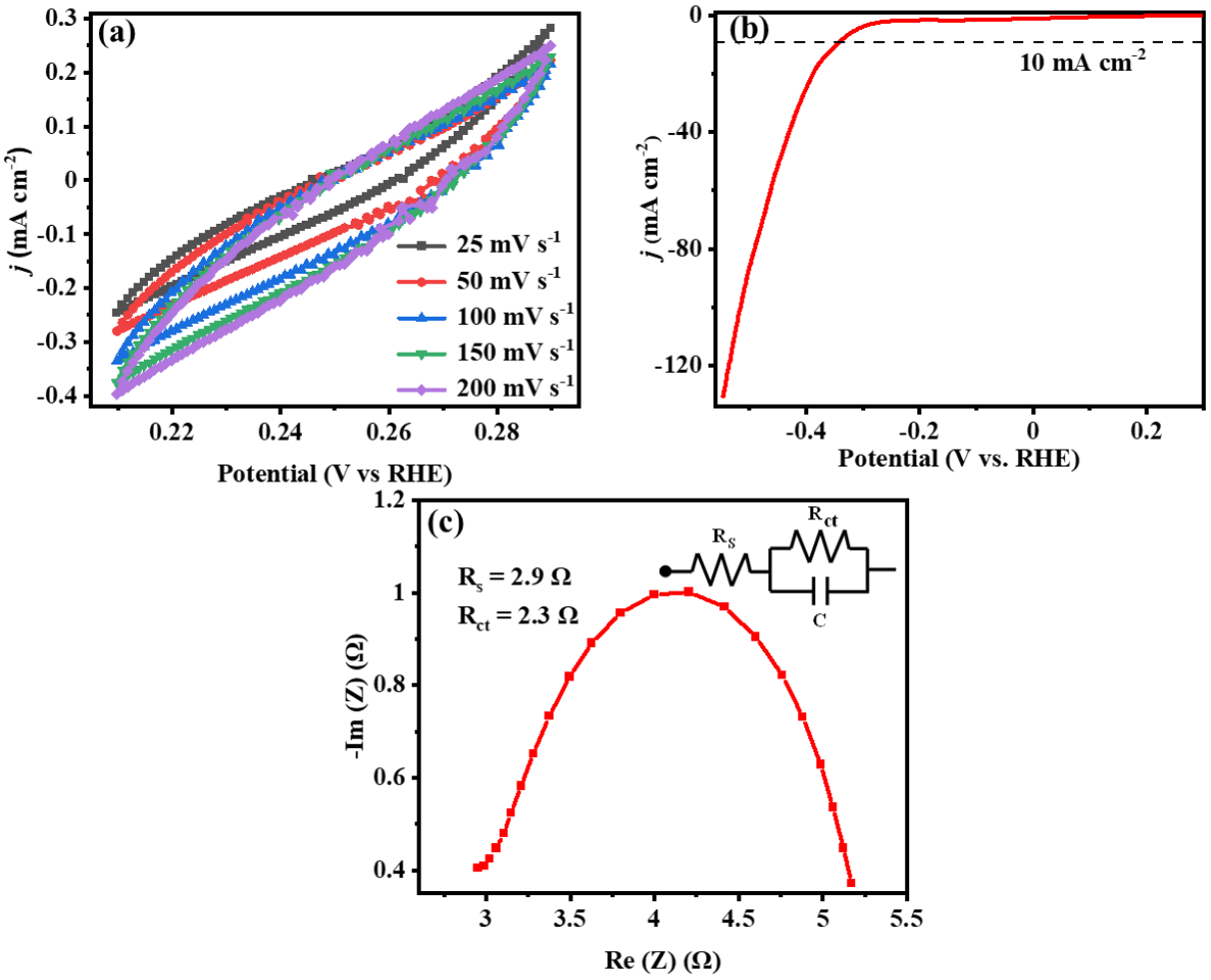

Figure S34. (a) Cyclic voltammetry (CV) at different scan rates (25, 50, 100, 150, and 200 mV s^{-1}) for C_{dl} and ECSA determination, (b) linear sweep voltammetry (LSV) curve and (c) Nyquist plot of PPA-2@12.

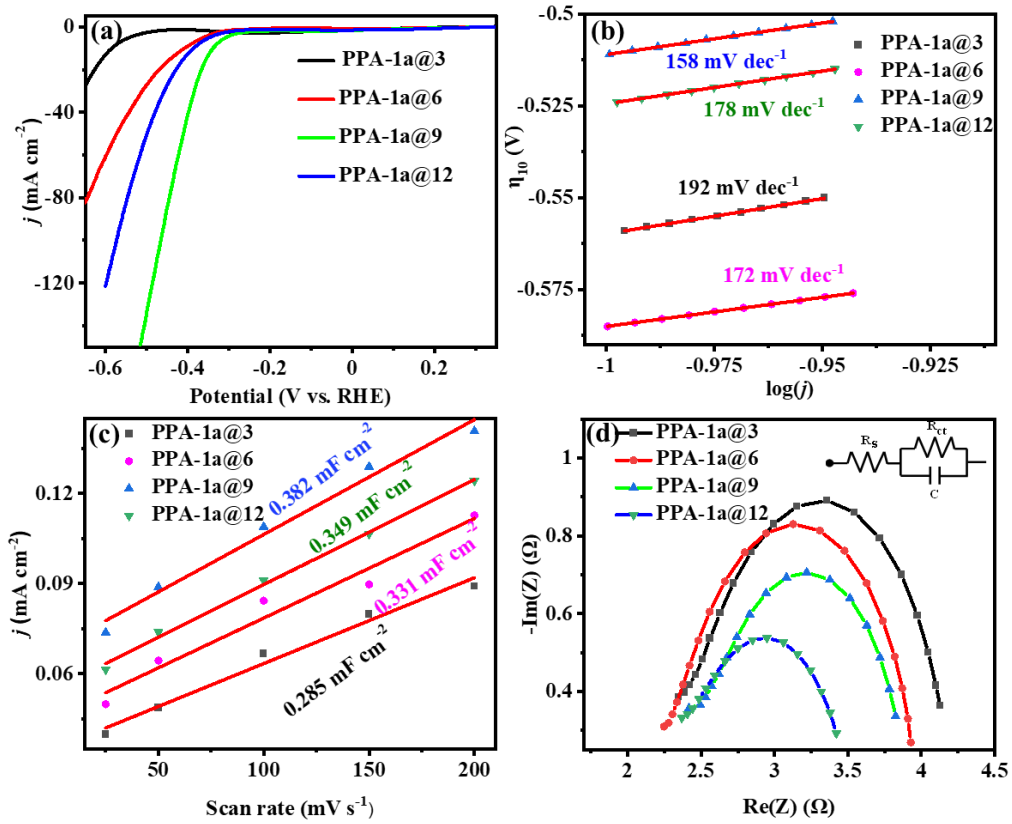

Figure S35. (a) Polarization curves (from LSV study in 0.5 M H_2SO_4, scan from 0 to -1.5 V Hg/$HgSO_4$ at a scan rate of 1 mV s^{-1}), (b) Tafel slopes, (c) Fitting C_{dl} values and (d) Nyquist plots of bare CC and CC loaded with different amount of PPA-1a (in mg).

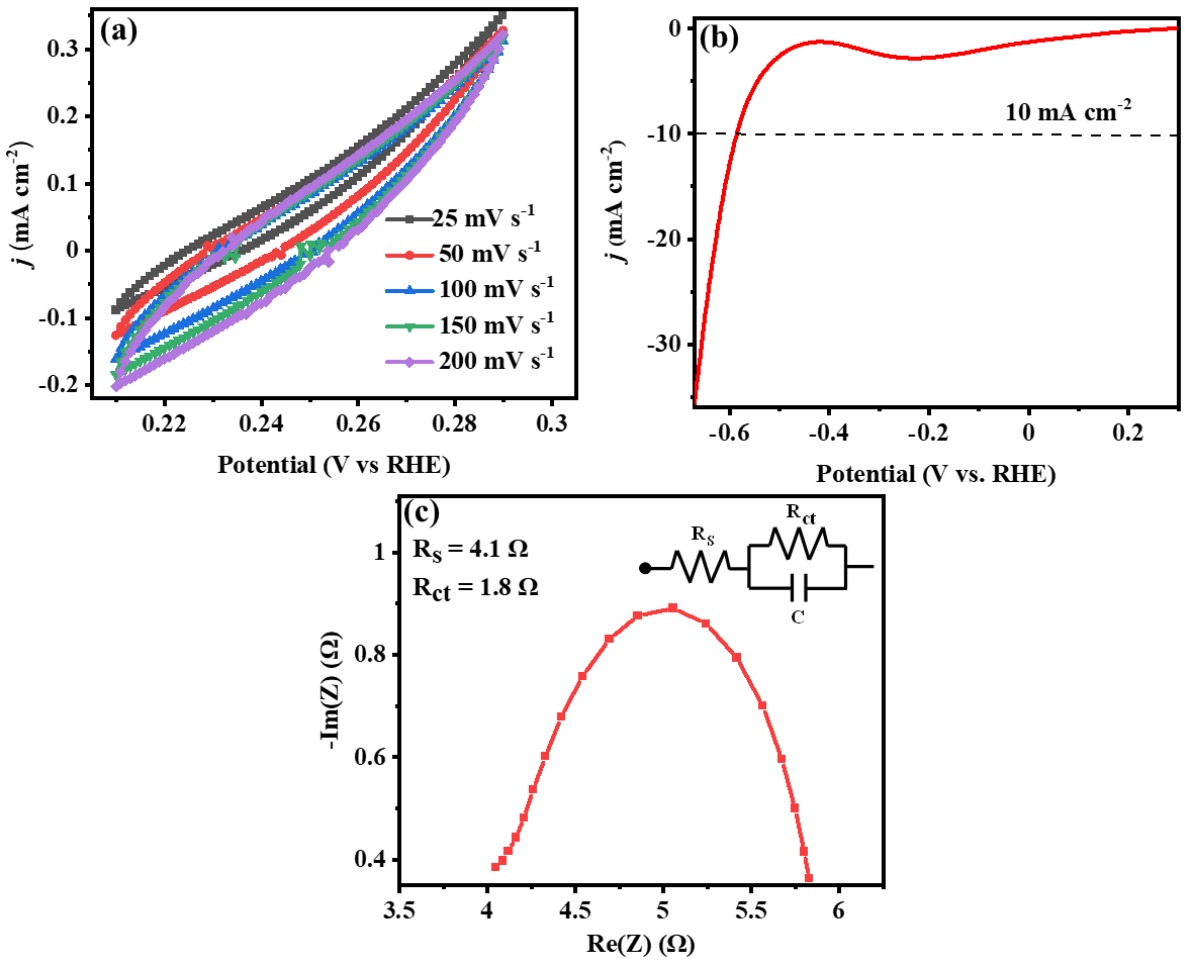

Figure S36. (a) Cyclic voltammetry (CV) at different scan rates (25, 50, 100, 150, and 200 mV s^{-1}) for ECSA and C_{dl} calculation, (b) Linear sweep voltammetry (LSV) curve and (c) Nyquist plot of PPA-1a@3.

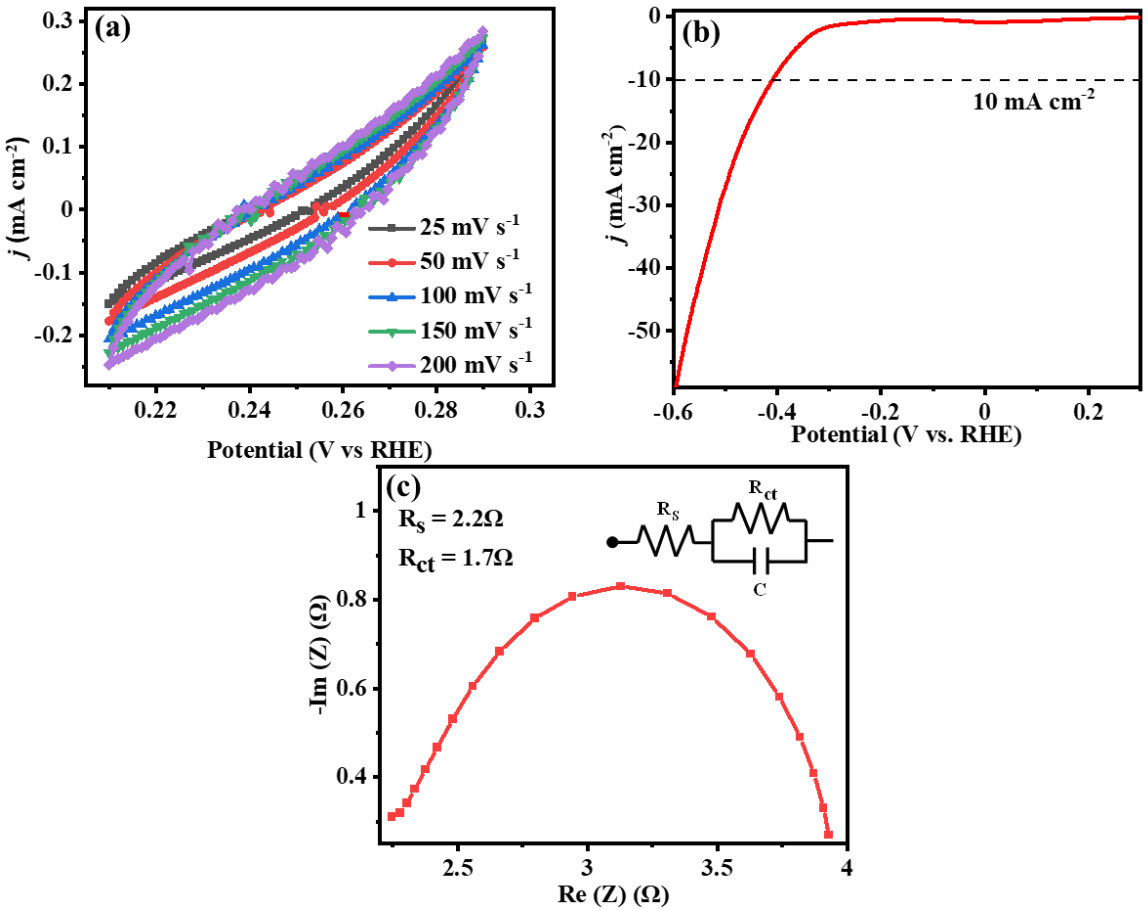

Figure S37. (a) Cyclic voltammetry (CV) at different scan rates (25, 50, 100, 150, and 200 mV s^{-1}) for ECSA and C_{dl} calculation, (b) linear sweep voltammetry (LSV) curve, and (c) Nyquist plot of PPA-1a@6.

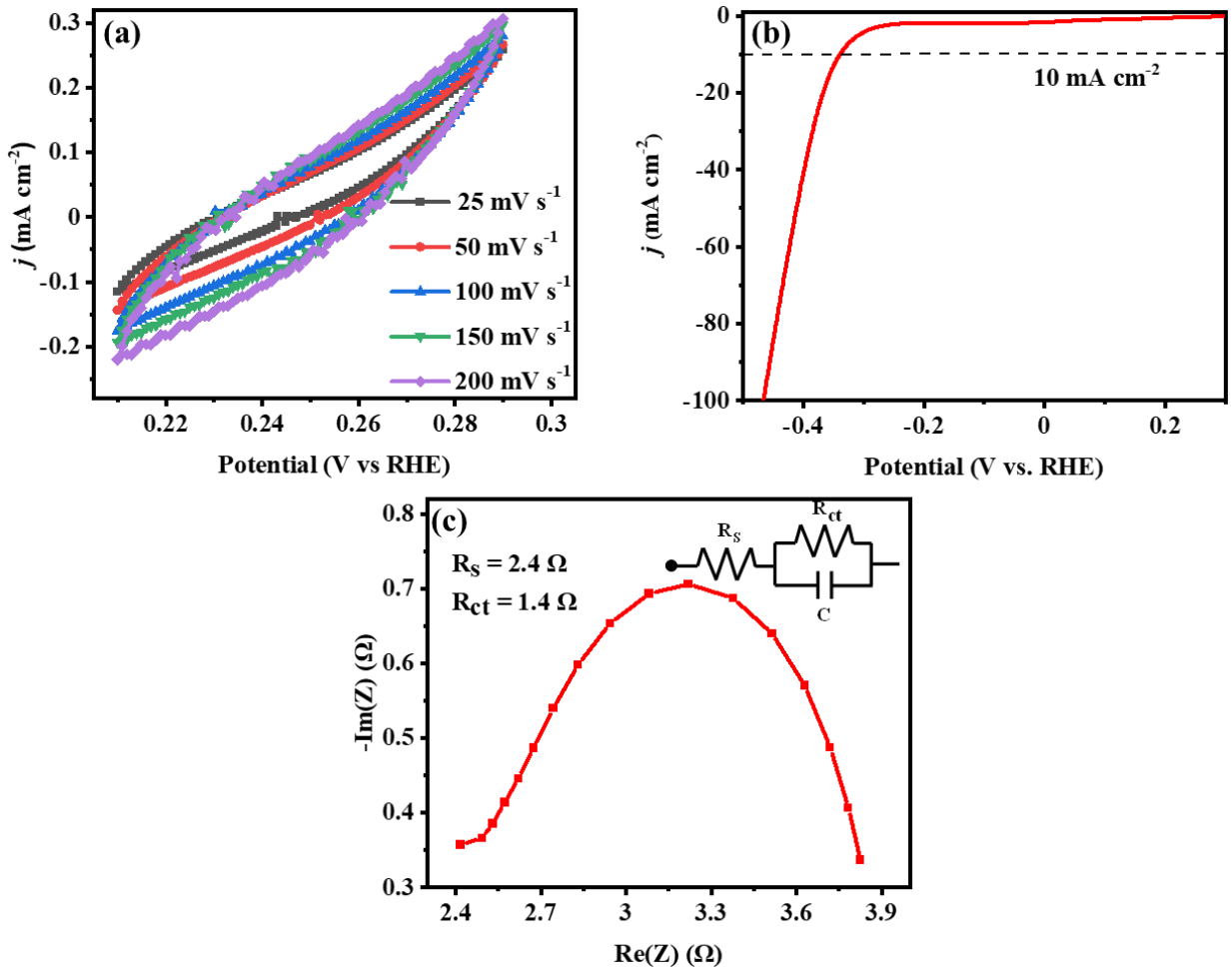

Figure S38. (a) Cyclic voltammetry (CV) at different scan rates (25, 50, 100, 150, and 200 mV s^{-1}) for ECSA and C_{dl} calculation, (b) linear sweep voltammetry (LSV) curve, and (c) Nyquist plot of PPA-1a@9.

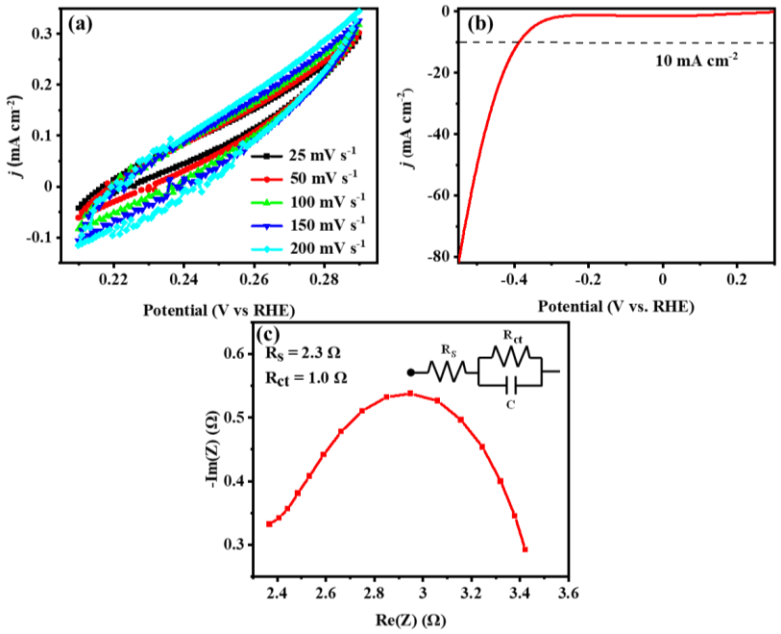

Figure S39. (a) Cyclic voltammetry (CV) at different scan rates (25, 50, 100, 150, and 200 mV s^{-1}) for ECSA and C_{dl} calculation, (b) linear sweep voltammetry (LSV) curve, and (c) Nyquist plot of PPA-1a@12.

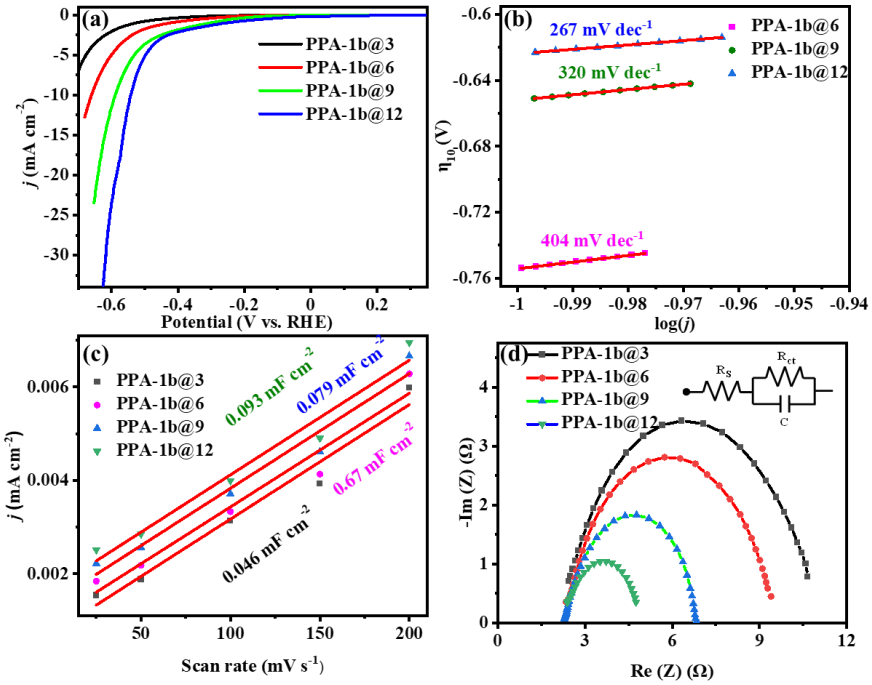

Figure S40. (a) Tafel slopes from the polarization curve (from LSV study in 0.5 M H_2SO_4, scan from 0 to -1.5 V vs $Hg/HgSO_4$ at a scan rate of 1 mV s^{-1}), (b) Fitting of C_{dl} values, and (c) Nyquist plots of CC and CC loaded with different amount of PPA-1b (in mg).

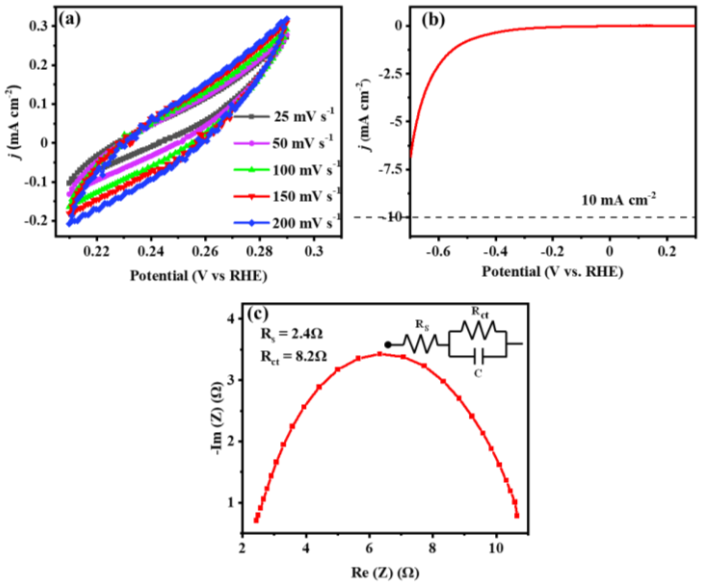

Figure S41. (a) Cyclic voltammetry (CV) at different scan rates (25, 50, 100, 150, and 200 mV s^{-1}) for ECSA and C_{dl} calculation, (b) Linear sweep voltammetry (LSV) curve, and (c) Nyquist plot of PPA-1b@3.

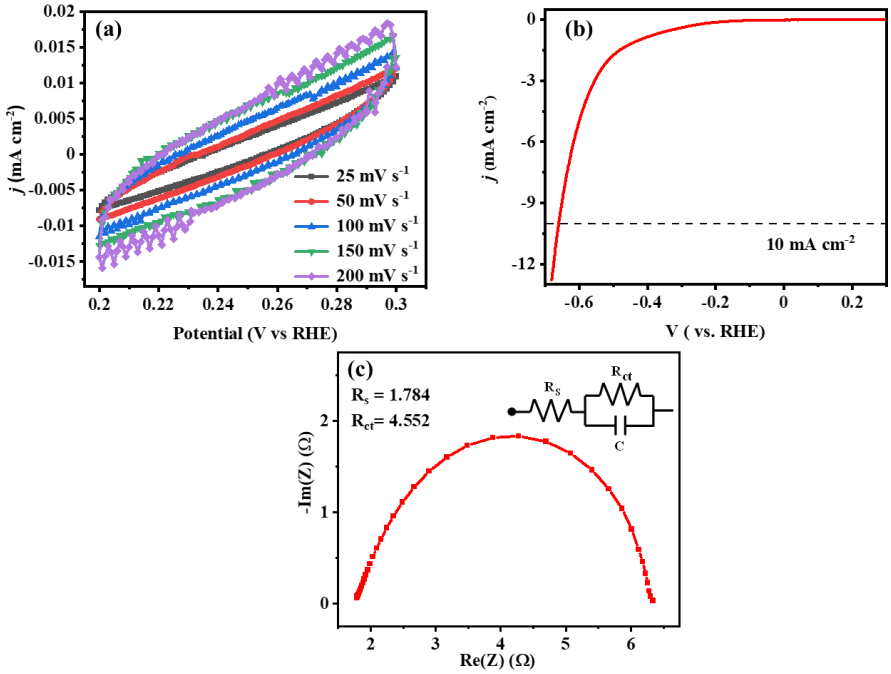

Figure S42. (a) Cyclic voltammetry (CV) at different scan rates (25, 50, 100, 150, and 200 mV s^{-1}) for ECSA and C_{dl} calculation, (b) linear sweep voltammetry (LSV) curve, and (c) Nyquist plot of PPA-1b@6.

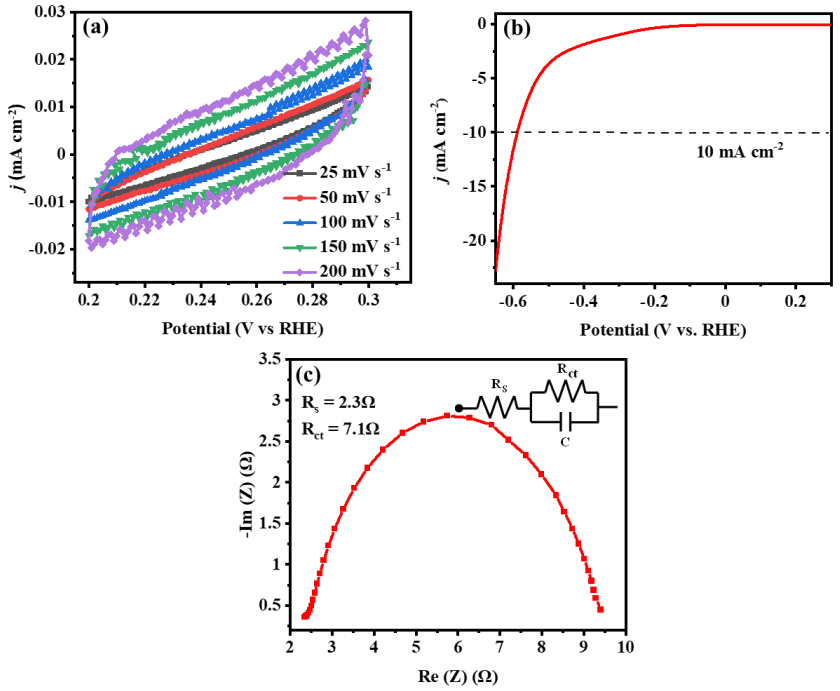

Figure S43. (a) Cyclic voltammetry (CV) at different scan rates (25, 50, 100, 150, and 200 mV s^{-1}) for ECSA and C_{dl} calculation, (b) linear sweep voltammetry (LSV) curve, and (c) Nyquist plot of PPA-1b@9.

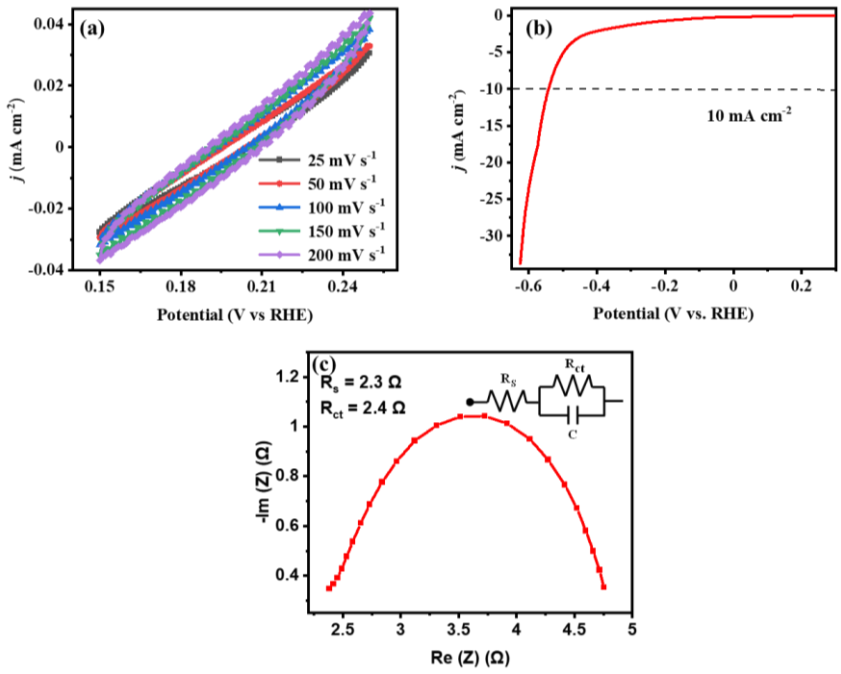

Figure S44. (a) Cyclic voltammetry (CV) at different scan rates (25, 50, 100, 150, and 200 mV s^{-1}) for ECSA and C_{dl} calculation, (b) linear sweep voltammetry (LSV) curve, and (c) Nyquist plot of PPA-1b@12.

Table S6. The overpotential, C_{dl} values, resistance, Tafel slopes and R_{ct} values of PPA-1a@x, PPA-1b@x, and PPA-2@x in 0.5 M H_2SO_4 electrolyte for HER study.

Sample	Overpotential (mV)	Tafel Slope ($mV\ dec^{-1}$)	C_{dl} Value ($mF\ cm^{-2}$)	R_{ct} (Ω)
PPA-1a@3	513	192	0.28	1.8
PPA-1a@6	459	172	0.33	1.7
PPA-1a@9	342	158	0.38	1.4
PPA-1a@12	368	178	0.35	1.0
PPA-1b@3	-	-	0.046	3.6
PPA-1b@6	754	404	0.067	2.5
PPA-1b@9	651	320	0.079	1.8
PPA-1b@12	626	267	0.093	3.01
PPA-2@3	545	174	0.98	9.6
PPA-2@6	394	169	1.09	4.6
PPA-2@9	318	143	1.19	4.2
PPA-2@12	353	166	1.16	2.4

Table S7. Comparative table of some recently reported materials for the performance of HER.

Electrode Materials	Overpotential ($mV@cm^{-2}$)	Tafel slope ($mV\ dec^{-1}$)	Electrolyte	Substrate	References
PPA-2	**318**	**143**	**0.5 M H_2SO_4**	**Carbon cloth**	**This work**
PPA-1a	**342**	**158**	**0.5 M H_2SO_4**	**Carbon cloth**	**This Work**
PPA-1b	**516**	**267**	**0.5 M H_2SO_4**	**Carbon cloth**	**This work**
TPOP	170	113	1M KOH	Nickel foam	[4]
(TpPAM)	250	106	0.5 M H_2SO4	Pt/C	[17]
DHI-PDA	190	80	1 M TfOH	Carbon Fiber paper	[18]
CoCOP	310	161	1.0 M KOH	Carbon Fiber paper	[19]
2DCCOF 1	541	130	0.5 M H_2SO_4 in water	Cu_2DCCOF1 film	[20]
$Co_3(BHT)_2$	340	149	0.5 M H_2SO_4 + 0.1 M KNO_3	GCE	[21]
THTNi 2DSP	330	80.5	0.5M H_2SO_4	RDE	[22]
2D CTGU-5	388	125	0.5 M H_2SO_4	GCE	[23]
NENU-500	237	96	0.5 M H2SO4	RDE	[24]
UiO-66-NH_2-Mo-5	200	59	0.5 M H_2SO_4	GCE	[25]
Co-THTA	283	71	0.5 M H_2SO_4	RDE	[26]
CuO@UiO-66	220	164	2 M KOH	Nickel foam	[27]

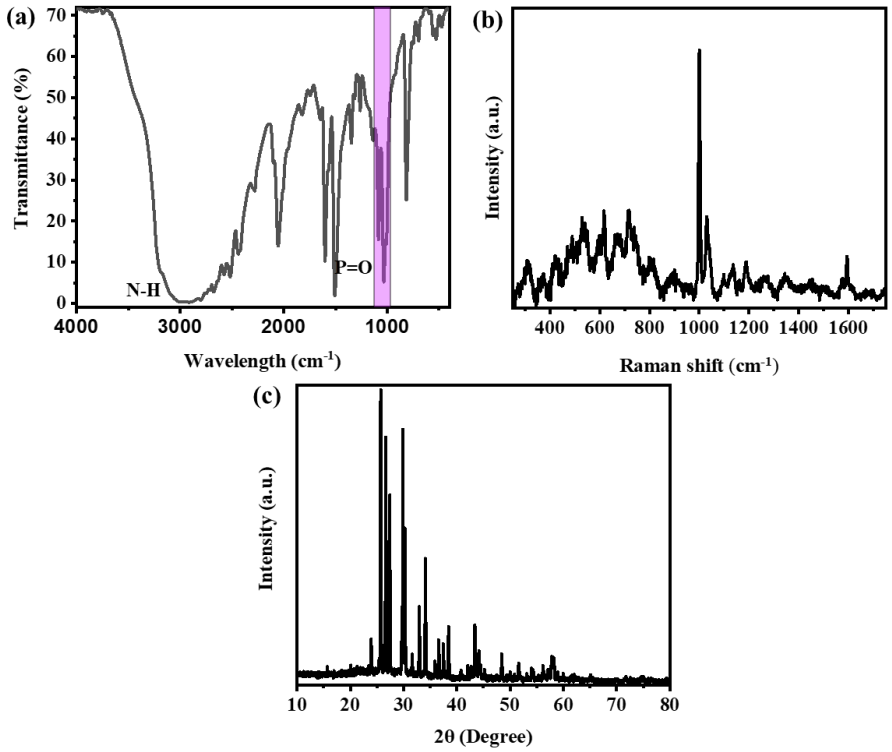

Figure S45. (a) FTIR spectrum, (b) Raman spectrum, and (c) PXRD analysis of PPA-2@9 before and after 10 h HER-CA analysis.

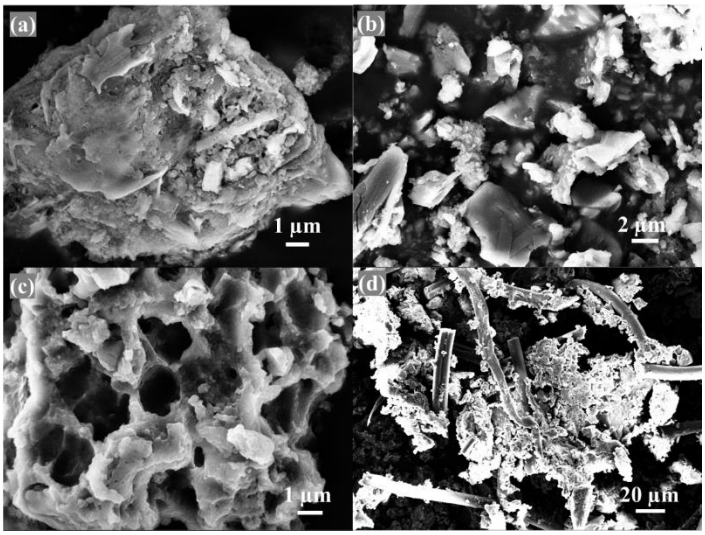

Figure S46. (a) FESEM images at different magnifications for PPA-2 after HER-CA study.

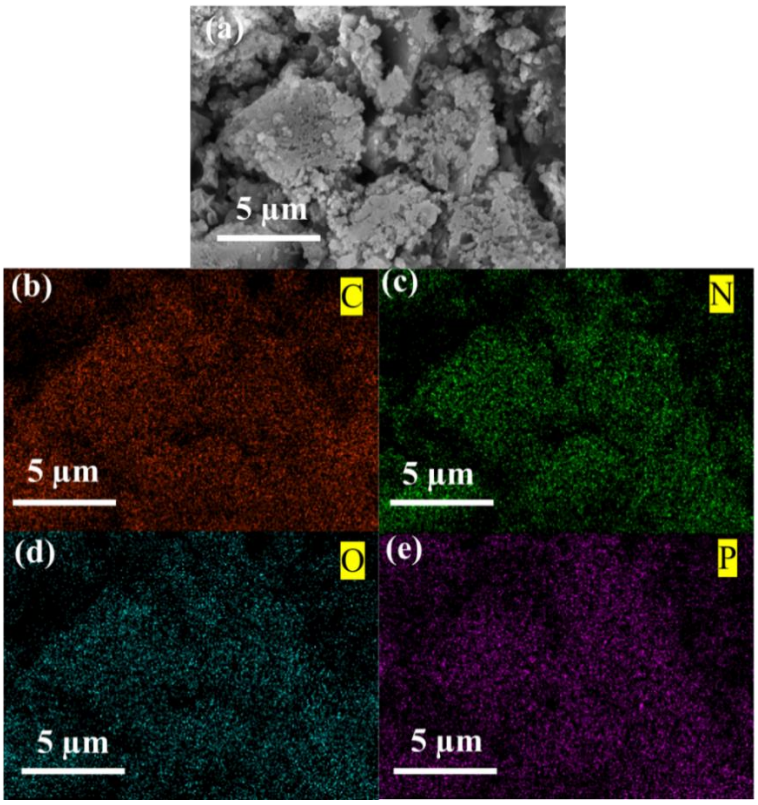

Figure S47. FESEM image of PPA-2@9 with the respective (b-e) EDX analysis after HER-CA analysis.

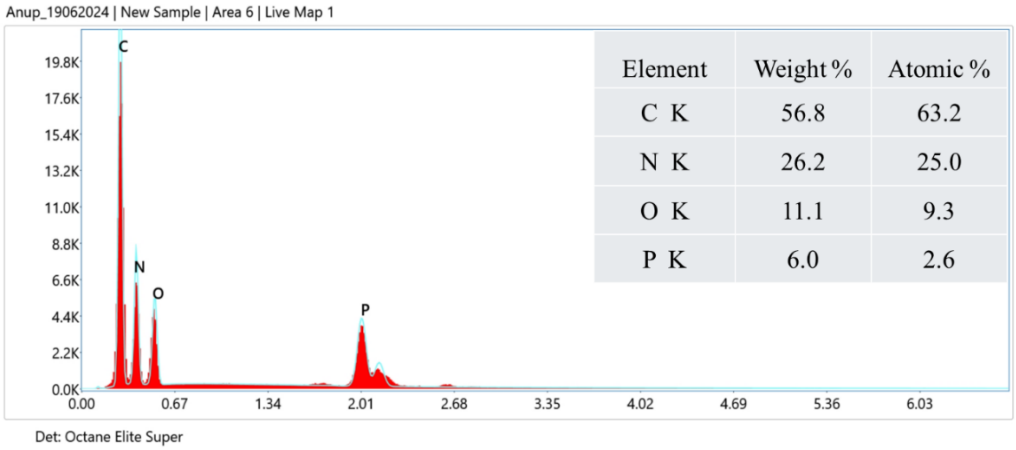

Element	Weight %	Atomic %
C K	56.8	63.2
N K	26.2	25.0
O K	11.1	9.3
P K	6.0	2.6

Figure S48. EDX spectrum of as-synthesized PPA-2 (Inset: the weight and atomic percentage of the present elements in PPA-2@9).

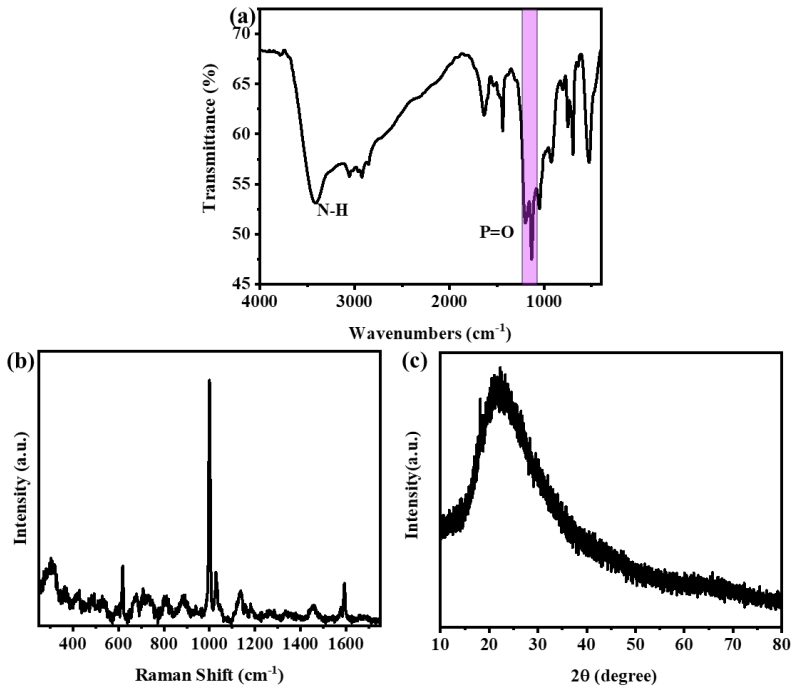

Figure S49. (a) FTIR spectrum, (b) Raman spectrmu, and (c) PXRD analysis of PPA-1a@9 before and after 10 h HER-CA analysis.

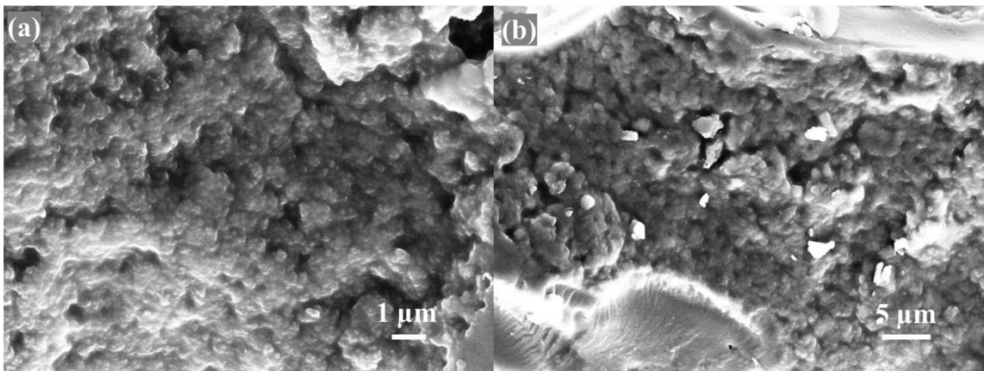

Figure S50. (a) FESEM images at different magnification for PPA-1a after HER-CA study.

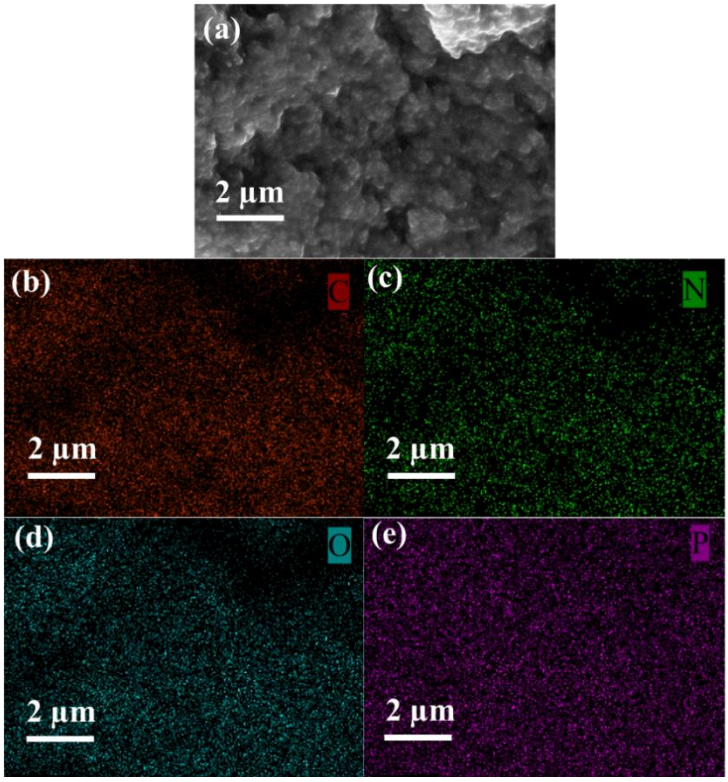

Figure S51. (a) FESEM image of PPA-1a@9 with the respective (b-e) EDX analysis after HER-CA analysis.

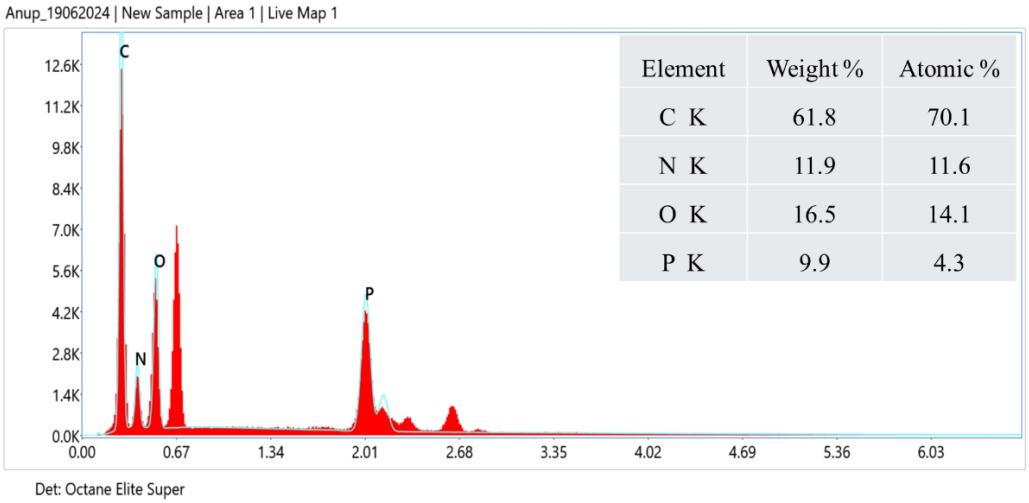

Element	Weight %	Atomic %
C K	61.8	70.1
N K	11.9	11.6
O K	16.5	14.1
P K	9.9	4.3

Figure S52. EDX spectrum of PPA-1a after HER-CA study (Inset: the weight and atomic percentage of the present elements in PPA-2@9).

Parameters (frequencies and energies) for Optimized structures of phosphamide.

Oxide form

Parameters	Values	Unit
Imaginary frequency		
Energy (RB3LYP)	-915.813717	Hartree
Electronic Energy (EE)	-915.813717	Hartree
Zero-point Energy correction	0.243153	Hartree
Thermal Correction to Energy	0.259860	Hartree
Thermal correction to Enthalpy	0.260804	Hartree
Thermal Correction to Free Energy	0.197754	Hartree
EE + Zero-point Energy	-915.570564	Hartree
EE + Thermal Energy Correction	-915.553857	Hartree
EE + Thermal Enthalpy correction	-915.552913	Hartree
EE + Thermal Free Energy Correction	-915.615963	Hartree
E (Thermal)	163.065	kcal/mol
Heat Capacity (Cv)	59.214	cal/mol-kelvin
Entropy (S)	132.700	cal/mol-kelvin

Oxonium form

Parameters	Values	Unit
Imaginary frequency	0	
Energy (RB3LYP)	-915.913418	Hartree
Electronic Energy (EE)	-915.913418	Hartree
Zero-point Energy correction	0.243139	Hartree
Thermal Correction to Energy	0.259847	Hartree
Thermal correction to Enthalpy	0.260791	Hartree
Thermal Correction to Free Energy	0.197751	Hartree
EE + Zero-point Energy	-915.670279	Hartree
EE + Thermal Energy Correction	-915.653571	Hartree
EE + Thermal Enthalpy correction	-915.652627	Hartree
EE + Thermal Free Energy Correction	-915.715667	Hartree
E (Thermal)	163.057	kcal/mol
Heat Capacity (Cv)	59.222	cal/mol-kelvin
Entropy (S)	132.680	cal/mol-kelvin

Ammonium form

Parameters	Values	Unit
Imaginary frequency	0	
Energy (RB3LYP)	-915.839472	Hartree
Electronic Energy (EE)	-915.839472	Hartree
Zero-point Energy correction	0.245415	Hartree
Thermal Correction to Energy	0.261451	Hartree
Thermal correction to Enthalpy	0.262395	Hartree

Thermal Correction to Free Energy	0.201441	Hartree
EE + Zero-point Energy	-915.594057	Hartree
EE + Thermal Energy Correction	-915.578021	Hartree
EE + Thermal Enthalpy correction	-915.577077	Hartree
EE + Thermal Free Energy Correction	-915.638031	Hartree
E (Thermal)	164.063	kcal/mol
Heat Capacity (Cv)	57.771	cal/mol-kelvin
Entropy (S)	128.290	cal/mol-kelvin

Iminium form

Parameters	Values	Unit
Imaginary frequency	0	
Energy (RB3LYP)	-915.906687	Hartree
Electronic Energy (EE)	-915.906687	Hartree
Zero-point Energy correction	0.243154	Hartree
Thermal Correction to Energy	0.259860	Hartree
Thermal correction to Enthalpy	0.260804	Hartree
Thermal Correction to Free Energy	0.197761	Hartree
EE + Zero-point Energy	-915.663533	Hartree
EE + Thermal Energy Correction	-915.646827	Hartree
EE + Thermal Enthalpy correction	-915.645883	Hartree
EE + Thermal Free Energy Correction	-915.708926	Hartree
E (Thermal)	163.065	kcal/mol
Heat Capacity (Cv)	59.212	cal/mol-kelvin
Entropy (S)	132.687	cal/mol-kelvin

Imine form

Parameters	Values	Unit
Imaginary frequency	0	
Energy (RB3LYP)	-915.851240	Hartree
Electronic Energy (EE)	-915.851240	Hartree
Zero-point Energy correction	0.243154	Hartree
Thermal Correction to Energy	0.259860	Hartree
Thermal correction to Enthalpy	0.260804	Hartree
Thermal Correction to Free Energy	0.197761	Hartree
EE + Zero-point Energy	-915.608086	Hartree
EE + Thermal Energy Correction	-915.591380	Hartree
EE + Thermal Enthalpy correction	-915.590436	Hartree
EE + Thermal Free Energy Correction	-915.653479	Hartree
E (Thermal)	163.059	kcal/mol
Heat Capacity (Cv)	59.217	cal/mol-kelvin
Entropy (S)	132.683	cal/mol-kelvin

Coordinates for Optimized structures of phosphamide.

Oxide form

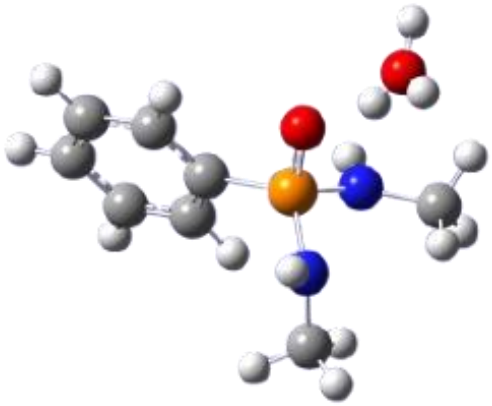

P	0.68746297	-0.15800278	0.14952491
N	1.11644607	-0.84212290	-1.30715894
H	0.66699827	-0.37224388	-2.09989802
C	-1.07139236	0.18254328	-0.04792925
C	-1.61132781	1.41724665	0.38495011
C	-1.94220517	-0.78669190	-0.57964416
C	-2.98502148	1.66713917	0.28224813
H	-0.95388718	2.17867576	0.78040262
C	-3.31440688	-0.52687292	-0.67846845
H	-1.54883698	-1.73888447	-0.91313378
C	-3.82542698	0.69481053	-0.24459492
H	-3.39607148	2.62264727	0.61093453
H	-3.98400304	-1.28045289	-1.09144850
H	-4.89417631	0.89097898	-0.31874890
N	1.01300829	-1.26973029	1.31417983
H	1.00127543	-0.83709256	2.24382079

C	2.56966710	-1.03021026	-1.50928063
H	3.11686126	-0.08118026	-1.57618616
H	2.99060622	-1.61760465	-0.69188171
C	0.30930051	-2.59989700	1.31185337
H	-0.74734353	-2.50935064	1.57223496
H	0.40208085	-3.06413783	0.34224253
H	2.73625174	-1.58136589	-2.43339821
H	0.78036039	-3.26477079	2.04353596
O	1.48122092	1.10091531	0.60665047
O	3.46755637	2.25617666	-0.03069540
H	4.25547409	1.51807731	0.59648155
H	3.54176418	3.46434596	0.34863215
H	2.44918112	1.86023155	0.17194461

Oxonium form

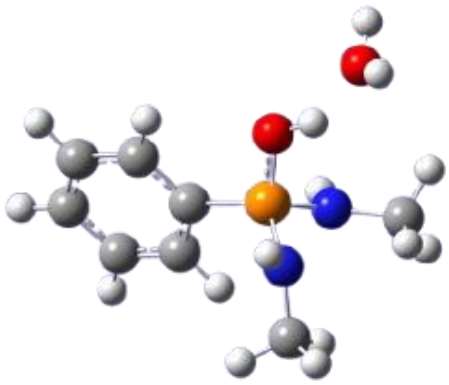

P	-0.62621855	0.00123807	0.01590370
N	-1.03058503	-0.96318392	1.27168342
H	-0.40394971	-0.92075809	2.06751302

C	1.16646730	0.16603721	0.07896640
C	1.77458912	1.41716233	-0.09375820
C	1.95815985	-0.98057840	0.24504745
C	3.16353334	1.51732687	-0.08819200
H	1.17033104	2.30505396	-0.22489096
C	3.34606772	-0.86933562	0.24738298
H	1.50054779	-1.95349461	0.37418580
C	3.94885378	0.37750125	0.08266140
H	3.63078608	2.48693569	-0.21462831
H	3.95429439	-1.75643810	0.37908372
H	5.02966055	0.46077612	0.08728981
N	-1.29589498	-0.69295225	-1.32649380
H	-1.38091603	-0.04697484	-2.10487900
C	-2.37075602	-1.50280089	1.55304339
H	-2.94409799	-0.83628059	2.20144555
H	-2.91720726	-1.64454230	0.62242816
C	-1.01820245	-2.08042786	-1.73809155
H	-0.01638780	-2.19629556	-2.16062793
H	-1.12569545	-2.75150354	-0.88736758
H	-2.26195336	-2.47182867	2.04066396
H	-1.75272535	-2.36439930	-2.49149228
O	-3.68035078	2.03791623	-0.08454891
H	-3.83705576	2.88400794	0.35740851
H	-3.97990057	2.17072072	-0.99440618
O	-1.15066628	1.49648096	0.01105092

H	-2.15123150	1.66491643	-0.04098430

Ammonium form

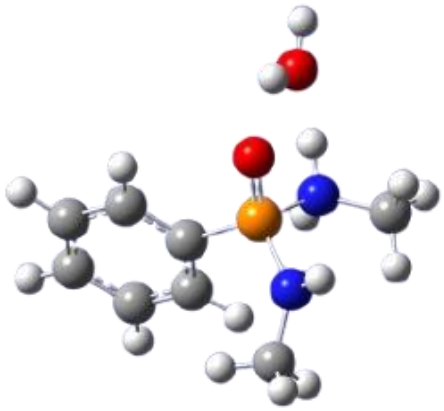

P	0.86632578	0.29671828	-0.62360013
N	1.70887782	-0.66133182	0.68674799
H	1.24023050	-1.58866568	0.69740268
C	-0.83670866	0.27355500	-0.16115503
C	-1.72377924	-0.15014309	-1.20302263
C	-1.32212835	0.54283518	1.09058694
C	-3.08758671	-0.24142194	-0.93633399
H	-1.35006971	-0.39057742	-2.19586718
C	-2.68059915	0.43199445	1.34889492
H	-0.63556824	0.81072299	1.88568712
C	-3.56442642	0.05226126	0.33869036
H	-3.77013843	-0.54446777	-1.72014128
H	-3.04987039	0.64423657	2.34427028
H	-4.62502279	-0.02148046	0.55040234

N	1.53394732	1.82265824	-0.58885593
H	2.44657527	1.88308709	-0.95551870
C	3.19239714	-0.79143510	0.55826415
H	3.39914956	-1.28060239	-0.39782174
H	3.67939924	0.15375742	0.62404295
C	1.25476019	2.78362173	0.56689069
H	1.64311027	3.75866874	0.27106666
H	0.17298023	2.89157375	0.72912056
H	3.52172326	-1.44873488	1.38036251
H	1.72425043	2.48269362	1.50350196
O	0.88749358	-0.80967786	-1.75123807
H	1.40533188	-0.38828803	1.65796655
O	0.49009458	-3.07299382	0.71445700
H	0.35171566	-2.75842567	-0.41397091
H	-0.26073752	-3.12978857	1.38560980

Iminium form

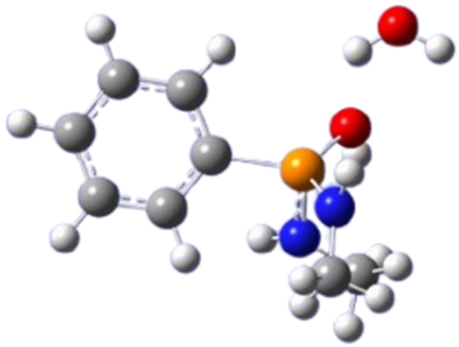

P	-0.71786844	-0.22660988	0.26516695
N	-0.97623062	-1.68799549	0.92877411
H	-0.22448634	-2.04930509	1.50545223

C	1.06800125	-0.01967244	0.16304670
C	1.64113034	1.23694052	0.40714464
C	1.87774724	-1.09477028	-0.23584704
C	3.01529911	1.40888206	0.26580369
H	1.02420264	2.07544607	0.70572931
C	3.25053915	-0.91033127	-0.37414795
H	1.44630261	-2.06681929	-0.43945221
C	3.81954275	0.33796620	-0.12253291
H	3.45548898	2.37973583	0.46036275
H	3.87374468	-1.74263202	-0.67917887
H	4.88898358	0.47688442	-0.23202924
N	-1.60227442	-0.13657800	-1.11875446
H	-1.79571332	0.81516408	-1.41597304
C	-2.28607056	-2.33618276	1.11153447
H	-2.67010564	-2.16650730	2.11933097
H	-2.99940418	-1.94311118	0.38967923
C	-1.41335541	-1.09058645	-2.22587204
H	-0.46325632	-0.94514503	-2.74659023
H	-1.46374626	-2.11193274	-1.85033646
H	-2.17651927	-3.40751126	0.94249479
H	-2.22983439	-0.94796682	-2.93295054
O	-1.33096966	1.05111736	1.03706436
H	-0.92499905	1.25295628	1.89605495
O	-2.55015546	3.38332151	-0.30961526
H	-3.50848379	3.27416239	-0.28384945

H	-2.20261416	2.60875983	0.15924373

Imine form

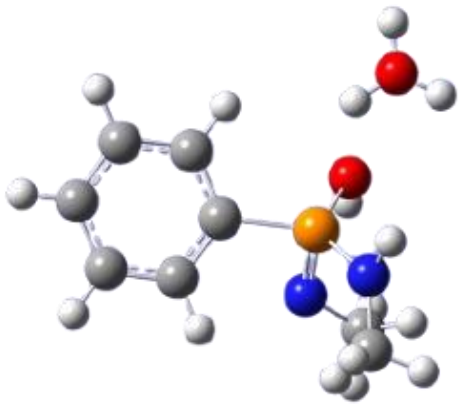

C	-2.90590855	-0.12302337	-1.14314740
C	-3.52244486	-0.75963674	-0.06358028
C	-2.75416811	-1.22670799	1.00325990
C	-1.36870939	-1.05927456	0.99448195
C	-0.74695591	-0.42129880	-0.08616151
C	-1.52256312	0.04689620	-1.15744994
H	-3.50024172	0.23896098	-1.97426809
H	-4.59848450	-0.89237735	-0.05564809
H	-3.23037722	-1.71985450	1.84290323
H	-0.77762186	-1.42253036	1.82675971
H	-1.05104026	0.53878496	-1.99995830
P	1.05451166	-0.28361703	-0.13896457
O	1.16525996	1.39162292	-0.44570602
H	2.07545175	1.70837459	-0.56553345
N	1.70552993	-0.39951980	1.37754708

H	2.38496680	-1.13653154	1.50867679
N	1.66139371	-1.22818404	-1.22362260
C	1.47872861	0.50193173	2.51094798
H	1.53861491	-0.06704845	3.43979635
H	2.21489904	1.31079884	2.54513503
H	0.48330999	0.94322856	2.45232403
C	3.10469564	-1.32442678	-1.46722735
H	3.66470163	-1.70108921	-0.60259680
H	3.27792602	-2.02388522	-2.28805417
H	3.55605405	-0.36849293	-1.76057938
H	-1.23383726	3.01676988	0.26438576
H	-0.09058700	4.06029200	-0.10775487
H	0.18812239	2.44296102	-0.39040482
O	-0.52326536	3.22250993	-0.38865971

References

1. W. J. Phang, W. R. Lee, K. Yoo, D. W. Ryu, B. Kim and C. S. Hong, *Angew. Chem. Int. Ed.*, 2014, **53**, 8383-8387.
2. N. C. Jeong, B. Samanta, C. Y. Lee, O. K. Farha and J. T. Hupp, *J. Am. Chem. Soc.*, 2012, **134**, 51-54.
3. F. Liu and K. Miyatake, *J. Mater. Chem. A*, 2022, **10**, 7660-7667.
4. M. Chaudhary, S. Kumar, L. Mallick and B. Chakraborty, *ACS Appl. Polym. Mater.*, 2023, **5**, 8235-8240.
5. C. Wang, H. Q. Li, Z. Wang, J. Xu, C. Liu, W. Liu, Z. Chen and X. Du, *Int. J. Hydrog. Energy*, 2020, **45**, 29738-29748.
6. S. Yuan, Q. Tang, B. He, H. Chen, Q. Li, C. Ma, S. Jin and Z. Liu, *J. Power Sources*, 2014, **249**, 277-284.
7. J. Zhang, S. Lu, H. Zhu, K. Chen, Y. Xiang, J. Liu, M. Forsyth and S. P. Jiang, *RSC Adv.*, 2016, **6**, 86575-86585.
8. R. Sahoo, S. Luo, N. K. Pendyala, S. Chand, Z.-H. Fu and M. C. Das, *Mater. Chem. Front.*, 2023, **7**, 3373-3381.

9. K. C. Ranjeesh, R. Illathvalappil, S. D. Veer, J. Peter, V. C. Wakchaure, Goudappagouda, K. V. Raj, S. Kurungot and S. S. Babu, *J. Am. Chem. Soc.*, 2019, **141**, 14950-14954.
10. V. R. Hande, S. K. Rath, S. Rao and M. Patri, *J. Membr. Sci.*, 2011, **372**, 40-48.
11. F. Wijaya, S. Woo, H. Lee, A. F. Nugraha, D. Shin and B. Bae, *J. Membr. Sci.*, 2022, **645**, 120203.
12. P. Sun, Z. Xia, Z. Li, Z. Fan, F. He, Q. Liu and X. Yin, *Mater. Today Chem.*, 2022, **23**, 100653.
13. D. H. Kim, I. K. Park and D. H. Lee, *Int. J. Hydrog. Energy*, 2020, **45**, 23469-23479.
14. A. Ghorai, S. Roy, S. Das, H. Komber, M. M. Ghangrekar, B. Voit and S. Banerjee, *ACS Appl. Polym. Mater.*, 2021, **3**, 4127-4138.
15. P. Ramaswamy, N. E. Wong, B. S. Gelfand and G. K. H. Shimizu, *J. Am. Chem. Soc.*, 2015, **137**, 7640-7643.
16. J. H. Lee, H. Kim, M. Kang, D. S. Choi and C. S. Hong, *Bull. Korean Chem. Soc.*, 2021, **42**, 322-325.
17. B. C. Patra, S. Khilari, R. N. Manna, S. Mondal, D. Pradhan, A. Pradhan and A. Bhaumik, *ACS Catal.*, 2017, **7**, 6120-6127.
18. H. Coskun, A. Aljabour, P. de Luna, H. Sun, N. Nishiumi, T. Yoshida, G. Koller, M. G. Ramsey, T. Greunz, D. Stifter, M. Strobel, S. Hild, A. W. Hassel, N. S. Sariciftci, E. H. Sargent and P. Stadler, *Adv. Mater.*, 2020, **32**, 1902177.
19. A. Wang, L. Cheng, W. Zhao, X. Shen and W. Zhu, *J. Colloid Interface Sci.*, 2020, **579**, 598-606.
20. H. Zhang, M. Zhu, O. G. Schmidt, S. Chen and K. Zhang, *Adv. Energy Sustainability Res.*, 2021, **2**, 2000090.
21. A. J. Clough, J. W. Yoo, M. H. Mecklenburg and S. C. Marinescu, *J. Am. Chem. Soc.*, 2015, **137**, 118-121.
22. L. Niu, L. Sun, L. An, D. Qu, X. Wang and Z. Sun, *MRS Bull.*, 2020, **45**, 562-568.
23. Y. P. Wu, W. Zhou, J. Zhao, W. W. Dong, Y. Q. Lan, D. S. Li, C. Sun and X. Bu, *Angew. Chem. Int. Ed.*, 2017, **56**, 13001-13005.
24. J. S. Qin, D. Y. Du, W. Guan, X. J. Bo, Y. F. Li, L. P. Guo, Z. M. Su, Y. Y. Wang, Y. Q. Lan and H. C. Zhou, *J. Am. Chem. Soc.*, 2015, **137**, 7169-7177.
25. X. Dai, M. Liu, Z. Li, A. Jin, Y. Ma, X. Huang, H. Sun, H. Wang and X. Zhang, *J. Phys. Chem. C*, 2016, **120**, 12539-12548.
26. R. Dong, Z. Zheng, D. C. Tranca, J. Zhang, N. Chandrasekhar, S. Liu, X. Zhuang, G. Seifert and X. Feng, *Chem. Eur. J.*, 2017, **23**, 2255-2260.
27. M. Fiaz, M. Athar, S. Rani, M. Najam-ul-Haq and M. A. Farid, *Mater. Chem. Phys.*, 2020, **239**, 122320.